

Isoxazole-Based-Scaffold Inhibitors Targeting Cyclooxygenases (COXs)

Maria Grazia Perrone,^[a] Paola Vitale,^[a] Andrea Panella,^[a] Savina Ferorelli,^[a] Marialessandra Contino,^[a] Antonio Lavecchia,^[b] and Antonio Scilimati^{*[a]}

A new set of cyclooxygenase (COX) inhibitors endowed with an additional functionality was explored. These new compounds also contained either rhodamine 6G or 6,7-dimethoxy-1,2,3,4-tetrahydroisoquinoline, two moieties typical of efflux pump substrates and inhibitors, respectively. Among all the synthesized compounds, two new COX inhibitors with opposite selectivity were discovered: compound 8 [*N*-(9-{2-[(4-{2-[3-(5-chlorofuran-2-yl)-4-phenylisoxazol-5-yl]acetamido}butyl)car-

bamoyl]phenyl-6-(ethylamino)-2,7-dimethyl-3*H*-xanthen-3-ylidene)ethanaminium chloride] was found to be a selective COX-1 inhibitor, whereas 17 (2-[3,4-bis(4-methoxyphenyl)isoxazol-5-yl]-1-[6,7-dimethoxy-3,4-dihydroisoquinolin-2-(1*H*)-yl]ethanone) was found to be a sub-micromolar selective COX-2 inhibitor. However, both were shown to interact with P-glycoprotein. Docking experiments helped to clarify the molecular aspects of the observed COX selectivity.

Introduction

Cyclooxygenase (COX)-1 and -2 isoforms share 60–65 % sequence identity within species, and about 85–90% sequence identity between different species.^[1] They are bifunctional enzymes that carry out two sequential reactions in spatially distinct but mechanistically coupled active sites: the bisoxygenation of arachidonic acid (AA) to prostaglandin G₂ (PGG₂), and the reduction of PGG₂ to PGH₂. COX-1 and COX-2 are homodimers of 70 kDa subunits, and dimerization is required for structural integrity and catalytic activity. Each monomer contains a COX and a peroxidase active site and consists of three structural domains: a short N-terminal epidermal growth factor domain, a membrane-binding domain, and a large, globular C-terminal catalytic domain. COX monomers forming the dimer, although identical in the resting enzyme, differ from one another during catalysis. *h*COXs function, in practice, as conformational heterodimers having a catalytic monomer (E cat) with a bound heme and an allosteric monomer (E allo) lacking heme. Studies of AA substrate turnover at high enzyme-to-substrate ratios indicate that non-substrate-like inhibitors bind the COX site of E allo to modulate the properties of E cat. The non-functioning subunit may provide structural support, enabling its partner monomer to catalyze COX reactions.^[2]

Interactions of varying complexities between ligands and (large) biomolecules (i.e., enzymes, DNA, receptors) are often studied using a simple model of ligand–biomolecule interac-

tions to determine the binding mode. For more complex systems, as in the case of COX E allo/E cat, the chance of observing a useful interaction for a randomly chosen compound decreases dramatically. We further explored these implications in the design of novel compounds in an attempt to potentiate the activity of our COX-1-selective inhibitors to develop therapeutic agents for in vitro and in vivo experiments targeting specific tissues and cells.^[3,4]

Traditional nonsteroidal anti-inflammatory drugs (tNSAIDs) target both COX isoenzymes. Coxibs, mainly targeting COX-2, have been the focus of several studies aimed at developing drugs lacking gastrointestinal toxicity. Conversely, few selective COX-1 inhibitors have been described, although a number of pharmacological investigations have proven the consolidated involvement of this enzyme in the carcinogenesis, pathogenesis of neuroinflammation, and pain.^[1] Nowadays, selective COX-1 inhibition is considered a promising therapeutic strategy in cancer and neuroinflammation-derived neurodegenerative diseases.^[1,5–7]

In many type of cancers and neurodegenerative diseases, drug efficacy strongly affects multidrug resistance (MDR),^[8] a phenomenon that limits drug cell accumulation due to efflux pump action, such as by P-glycoprotein (P-gp), a key member of the superfamily of ATP-binding cassette (ABC) efflux transporters. This prompted us to design suitable selective COX-1 inhibitors^[1,3–5,9] that were also capable of residing for a longer time inside the cell. Until now, no attempt to correlate COX-1 and P-gp activity has been successful.

Hence, the new projected compounds have a COX inhibitor recognition moiety, constituted by one of three well-known selective inhibitors such as indomethacin,^[10] P6,^[3,11] or mofezolac^[12] (Figure 1), and a P-gp-recognized fragment as a further functionality. Notably, rhodamine 6G (Rh6G) is a P-gp substrate, and 6,7-dimethoxy-1,2,3,4-tetrahydroisoquinoline (6,7-DM-

[a] Dr. M. G. Perrone,* Dr. P. Vitale,* Dr. A. Panella, Prof. S. Ferorelli, Dr. M. Contino, Prof. A. Scilimati
Dipartimento di Farmacia—Scienze del Farmaco
Università degli Studi di Bari “A. Moro”, Via E. Orabona 4, 70125 Bari (Italy)
E-mail: antonio.scilimati@uniba.it

[b] Prof. A. Lavecchia
Dipartimento di Farmacia, “Drug Discovery” Laboratory
Università di Napoli “Federico II”, Via D. Montesano 49, 80131 Napoli (Italy)

[*] These authors contributed equally to this work.

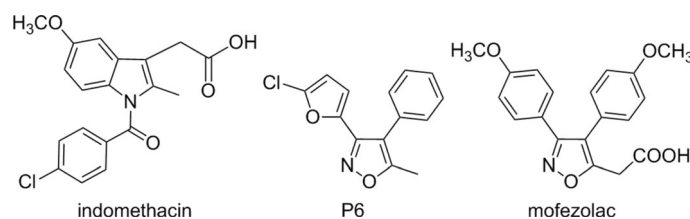


Figure 1. Structures of indomethacin, P6, and mofezolac.

THIQ) is a structural key element of elacridar and tariquidar (two P-gp saturating substrates or inhibitor-like compounds).^[13–16] Indomethacin, P6, and mofezolac were then linked to either a Rh6G or 6,7-DM-THIQ moiety to first explore the COX inhibitor recognition and, secondly, to verify if such new molecules retain P-gp substrate/inhibitor activity.

A series of conformationally restricted and regioisomeric indomethacin analogues were already described as multidrug-resistant modulators. Evaluation of the inhibitory effects of these compounds on COX, P-gp, and multidrug resistance (MDR) indicated that modulation of multidrug-resistant P-gp and multidrug-resistant protein 1 by a number of NSAIDs is not associated with COX-1 and COX-2 inhibitory activities.^[17] Ibuprofen overcame MDR in human doxorubicin-resistant uterine sarcoma cells (MES-SA/Dx-5), expressing high levels of efflux pump P-gp.^[18] Rh6G was also conjugated with indomethacin, P6, and mofezolac in an attempt to produce fluorescent molecules targeting COX-1 expressed in healthy and pathological tissues/cells.

Herein we report the synthesis of these original compounds, their ability to inhibit COX activity, and their extent of interaction with the P-gp efflux pump expressed in the MDCK-MDR1 cell line. Results of the docking experiments are also discussed.

Results and Discussion

Among tNSAIDs, other than low-dose Aspirin, only a few examples of selective COX-1 inhibitors have been investigated in depth thus far.^[1] For this study, we identified novel compounds

derived from leads such as indomethacin (COX-1 IC_{50} = 0.099 mm; COX-2 IC_{50} = 4.2 mm),^[9] P6 (COX-1 IC_{50} = 22 mm; COX-2 IC_{50} > 50 mm),^[3] and mofezolac^[11] (COX-1 IC_{50} = 0.024 mm; COX-2 IC_{50} > 50 mm) (Figure 1) to further identify crucial chemical entities responsible for COX selective inhibition.

Indomethacin was chosen as one of the most prescribed analgesic and antipyretic tNSAIDs. Mofezolac is the active ingredient of the analgesic drug Disopain, commercially available in Japan. P6 represents a prototype of the isoxazole scaffold we have been studying.^[5,19,20]

P6 was converted into P6-COOH (Figure 2; 32 and 58 % inhibition of COX-1 and COX-2 activity, respectively, at 50 mm) by adding the carboxylic group to the P6 isoxazole side chain.^[19]

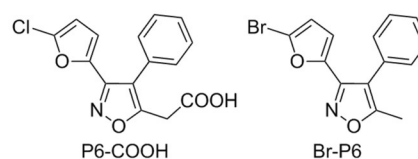


Figure 2. Structures of P6-COOH and Br-P6.

All three COX inhibitors (indomethacin, P6-COOH, and mofezolac) were linked to the fluorescent fragment Rh6G^[21] or to the efflux-pump-interacting moiety 6,7-DM-THIQ,^[14] obtaining compounds 7–9, 14–17, and 20 (Tables 1 and 2, and Schemes 2 and 4–6).

The COX-1 inhibitor portion of the compounds and the Rh6G or 6,7-DM-THIQ moieties were coupled by a linker of the appropriate length^[21,22] to first allow the entrance of the COX-1-inhibitor portion into the COX active site to reach the tyrosyl radical (Tyr 385) (Figure 3)^[21,22] and hence block the auto-catalytic oxidation of AA to PGH₂. Second, the linker length was selected so as to allow the additive Rh6G or 6,7-DM-THIQ functionality to remain outside of the constriction site formed by Tyr 355, Arg 120, and Glu 524 (Figure 3 a). The same amino acid residues allow easier access to the COX-2 active site, which has a larger side pocket than the COX-1 isoform (Figure 3 b). Target

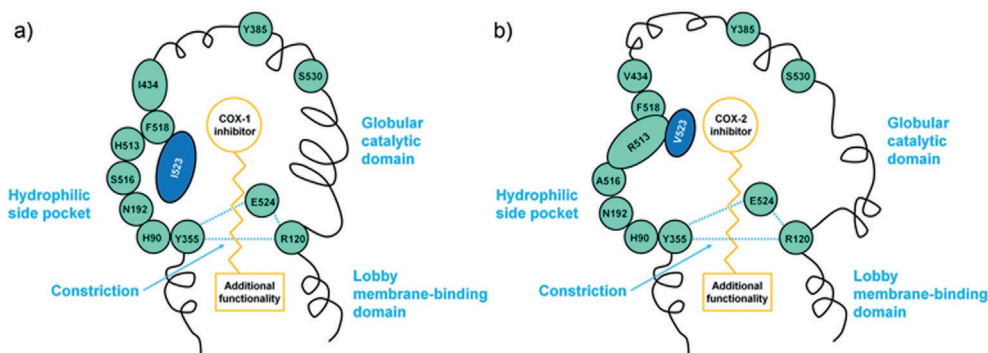


Figure 3. Working hypothesis: target molecules in the a) COX-1 and b) COX-2 active sites. COX-1 and COX-2 active sites are schematically depicted as narrow hydrophobic channels separated from the residual protein, partly consisting of the wide lobby of the membrane-binding domain with a constriction site composed of three amino acids (Arg 120, Tyr355, and Glu 524). The channel is located at the interface between the region that penetrates the membrane and the catalytic region. For the COX-1 isoform, Ile 523 (blue) closes the hydrophilic side pocket located laterally. In the COX-2 isoform, there is a more accessible pocket. There is a wider channel opening in COX-2, with narrowing caused by Arg 120 and Tyr355 in COX-1.

Table 1. Fragment-based construction of target compounds 7–9 and 14–17, derived from indomethacin, P6-COOH, and mofezolac.

Compound	COX-1-recognized fragment	R ¹ (linker)	R ² (additive functionality)
7			
8			
9			
14			
15			
16			
17		–	

compound 17, linking the COX inhibitory and 6,7-DM-THIQ moieties, was used to test the role of the linker in this series and to identify structural features to design novel selective COX inhibitors.

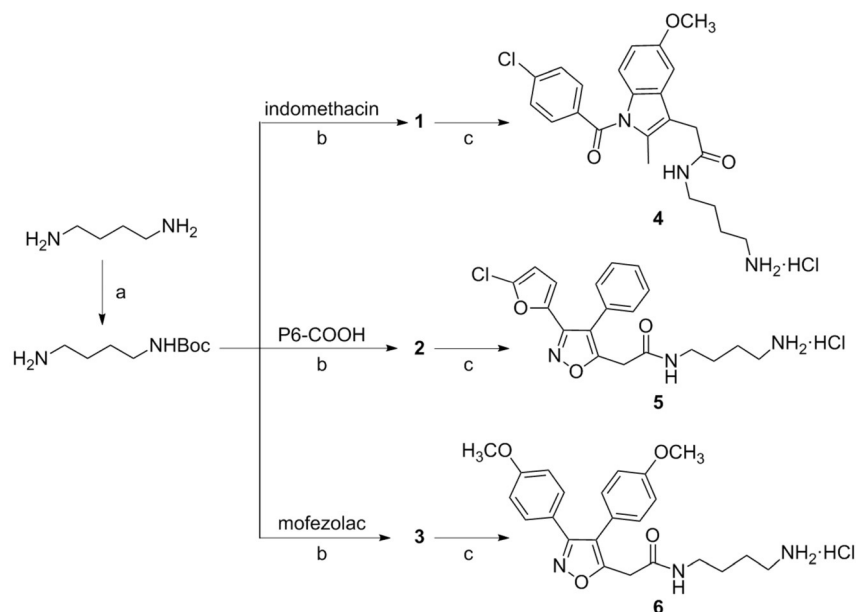
Chemistry

Syntheses of 1–3 were accomplished by an amide bond formation between the corresponding one of the three COX inhibitors and a diamine, which was used as a linker. Mono-*N*-Boc protection of 1,4-diaminobutane afforded the corresponding *tert*-butyl (4-aminobutyl)carbamate^[23] (Scheme 1), which in turn reacted with in situ EDCI/HOBt-activated indomethacin, P6-COOH, and mofezolac (Scheme 1) to give mono-*N*-Boc adducts 1–3.

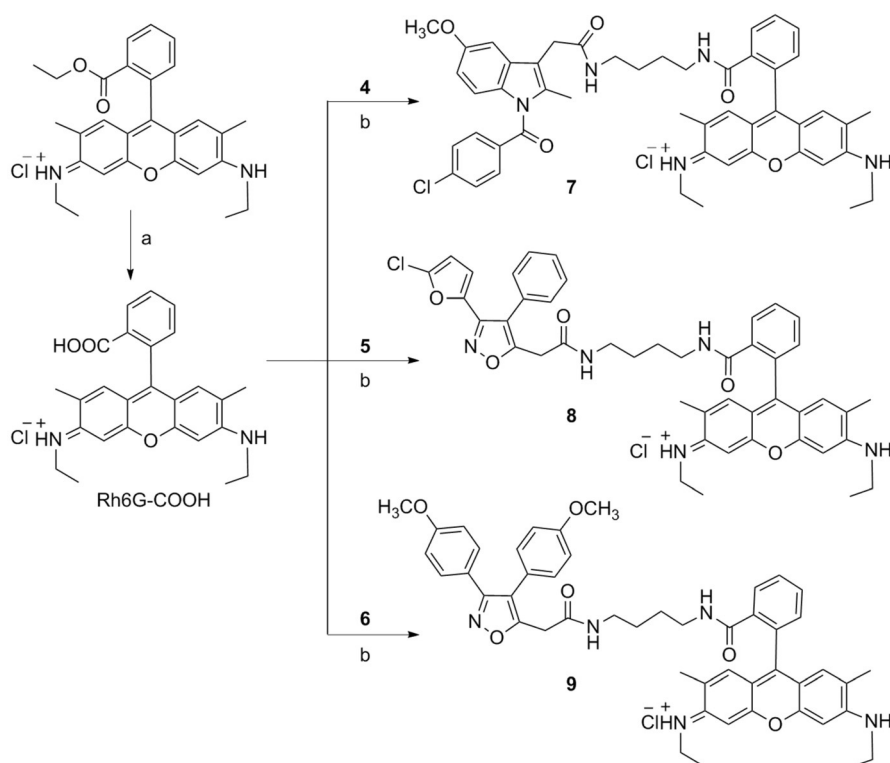
The *N*-Boc deprotection of 1–3, precursors of 4–6, was performed in high yield (92–98 %) by HCl_(g). The subsequent conjugation of 4–6 with the rhodamine moiety (Rh6G-COOH) led

to target compounds 7–9 (Scheme 2). Rh6G-COOH was obtained by hydrolysis of the commercially available Rh6G (ethyl ester) in the presence of NaOH.^[24]

Target compounds 14–16 were prepared from 5-amino-1-[6,7-dimethoxy-3,4-dihydroisoquinolin-2-(1*H*)-yl]pentan-1-one hydrochloride (13) by reacting the 6,7-DM-THIQ (11) with *N*-Boc-protected 5-aminovaleric acid (10),^[25] activating in situ with EDCI/HOBt, followed by deprotection with HCl_(g) (Scheme 3). The subsequent conjugation of 13 with indomethacin, P6-COOH, or mofezolac led to target compounds 14–16 (Scheme 4). Target compound 17, obtained by conjugating mofezolac and 6,7-DM-THIQ (11), was prepared to verify the importance of the distance between the COX-1 inhibitor portion and 6,7-DM-THIQ (Scheme 5). The first synthetic conditions (Scheme 6) used to prepare 14 resulted in cleavage of the 4-chlorobenzoyl group, thus obtaining compound 20, which was included in the pharmacological characterization (Table 2).



Scheme 1. Reagents and conditions: a) di-*tert*-butyl dicarbonate, dioxane, RT; b) DIEA, EDCI, HOBT, dry DMF, RT, overnight; c) $\text{HCl}_{(\text{g})}$, dry CH_2Cl_2 , RT, 1.5 h.

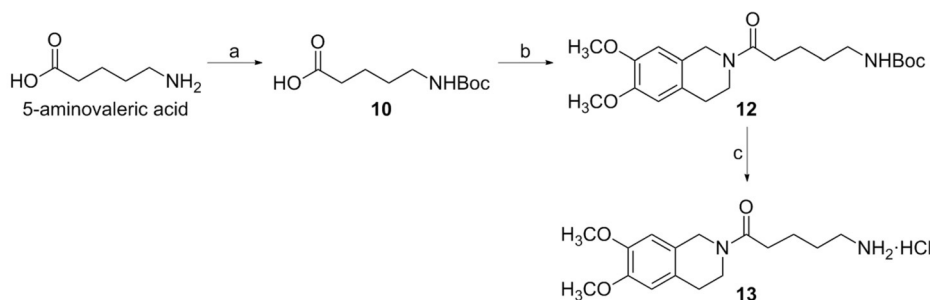


Scheme 2. Reagents and conditions: a) $\text{NaOH}_{(\text{aq})}$, EtOH, reflux, overnight; b) PyBOP, TEA, $\text{CH}_2\text{Cl}_2/\text{DMSO}$, RT, 24 h.

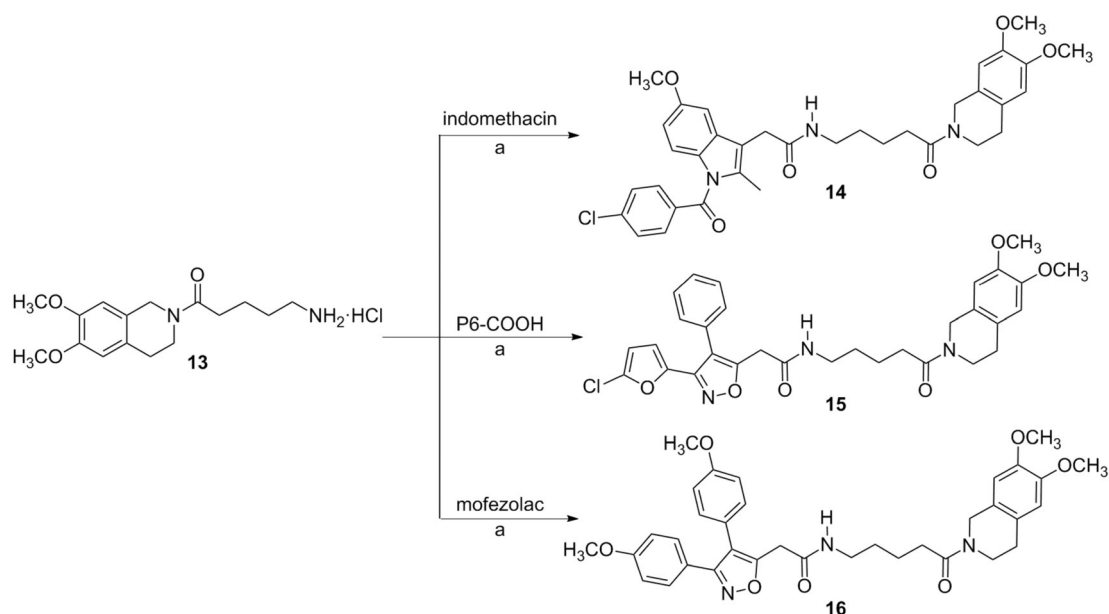
Biology

All synthesized compounds were tested to determine their inhibitory activity toward the COX-1 and COX-2 enzymes, respectively (Table 2), using a colorimetric COX (ovine) inhibitor screening assay kit. COX is a bifunctional enzyme that exhibits both cyclooxygenase and peroxidase activity.

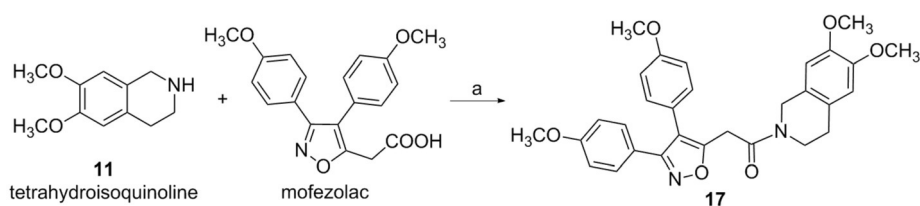
Indomethacin selectively inhibited COX-1 with $\text{SI} = 0.02$ (Table 2). Rh6G-COOH did not inhibit COXs activity at 50 μM . A combination of indomethacin and Rh6G-COOH, with a 1,4-diaminobutane linker, afforded 7, which was not able to inhibit COX-1, although it decreased COX-2 activity at 50 μM by 28 %. On the other hand, 8 was found to be highly COX-1-selective, with $\text{IC}_{50} = 6.0 \mu\text{M}$ and a total lack of efficacy toward COX-2 at



Scheme 3. Reagents and conditions: a) di-tert-butyl dicarbonate, dioxane, RT; b) 6,7-DM-THIQ (11), DIPEA, EDCI, HOBT, dry DMF, RT, 20 h; c) HCl_(g), dry CH₂Cl₂, RT, 1.5 h.



Scheme 4. Reagents and conditions: a) DIPEA, EDCI, HOBT, dry DMF, RT, 20 h.

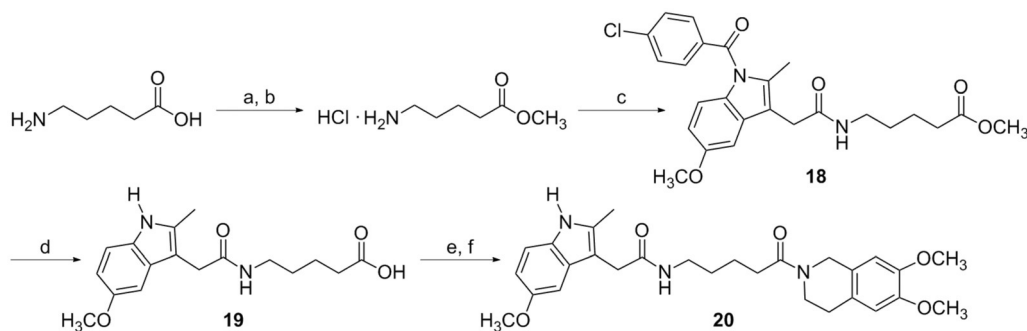


Scheme 5. Reagents and conditions: a) DIEA, EDCI, HOBT, dry DMF, RT, overnight.

concentrations up to 50 μ M, although it was found that conjugation of the Rh6G moiety with P6 to afford compound 8 results in a loss of fluorescence (data not shown). Compound 9 was found to be a poor inhibitor, with activity only toward COX-1 (16 % inhibition at 50 μ M).

Within the series of 6,7-DM-THIQ derivatives, indomethacin derivative 14 was completely inactive toward both COX isoforms, and its analogue (20) showed only 10 % inhibition of COX-1. Compound 15, derived from P6-COOH, slightly affected

only COX-1 activity (23 % inhibition at 50 μ M). Mofezolac derivative 16, at a concentration of 50 μ M, showed 33 and 13 % inhibition of COX-1 and COX-2, respectively. The common structural element in all of the target compounds was the approximate distance between the COX and P-gp binding fragments. This was chosen based on the results obtained from building fluorescent imaging agents for the selective visualization of COX-2 in inflammation and cancer.^[21,22] Such a linker length proved to be suitable to allow 8 to have the P6 moiety close



Scheme 6. Reagents and conditions: a) SOCl_2 , 0°C ; b) anhydrous CH_3OH , reflux; c) indomethacin, HOBt, DCC, DIEA/anhydrous CH_2Cl_2 ; d) LiOH , THF, RT; e) DCC, DMAP (0°C , 30 min)/anhydrous CH_2Cl_2 ; f) 6,7-DM-THIQ (11), 16 h, RT.

to the Tyr 385 residue in the COX-1 catalytic site and the bulky Rh6G moiety in proximity of the entrance of the long hydrophobic channel of the COX membrane-binding domain (Figure 4). In the absence of a linker, as with compound 17, 48% and 69% inhibition of COX-1 and COX-2 activity, respectively, were observed at a concentration of 50 μM (COX-2 $\text{IC}_{50} = 0.95 \mu\text{M}$).

Docking studies

The COX active site of both COX-1 and COX-2 is located at the terminus of a long hydrophobic channel that runs from the protein surface to the interior of the protein (Figure 3). The initial portion of the channel has a large volume, or lobby, which narrows at a constriction site composed of residues Arg 120, Tyr 355, and Glu 524. The constriction site constitutes a gate that must open and close for substrates and inhibitors to pass into or out of the above-located COX active site. All COX inhibitors bind in the active site above the constriction site, and the constriction site residues play an important role in binding carboxylic acid-containing inhibitors through a combination of ion pairing and hydrogen bonding.^[26]

To gain more insight into the probable nature of the binding interactions of compound 8 within the active site of COX-1, docking studies were conducted using the ovine COX-1 in complex with bound inhibitor indomethacin-(*R*)- α -ethyl-ethanolamide (PDB ID: 2OYE).^[27] This crystal structure was selected, because the side chain of Arg 120 adopts a significantly altered conformation to accommodate the inhibitor, relative to the more extended conformation observed in most other COX-1 crystal structures. One consequence of this structural readjustment is the disruption of the Arg 120–Tyr 355–Glu 524 constriction site and potential expansion of the entrance to the main hydrophobic channel.

Docking investigations were carried out using the GOLD 5.2.2 automated docking program^[28,29] in combination with the ChemPLP scoring function, followed by rescoring with ChemScore.^[3,19,30–34] Alternative conformations of the Arg 120, Tyr 355, Glu 524, and Ser 530 side chains have been previously observed in COX crystal structures complexed with several inhibitors, highlighting the innate plasticity of the active site.^[26,35,36] Accordingly, the Arg 120, Tyr 355, Glu 524, and

Ser 530 side chains were allowed to move during the docking experiments.

An initial validation of the docking protocol was performed by comparing the conformation, position, and orientation (pose) of the inhibitor indomethacin-(*R*)- α -ethyl-ethanolamide, as obtained from docking with the one experimentally determined X-ray crystal structure. Correctly re-docking the crystallographically observed inhibitor was a minimum requirement to determine whether the program was applicable to this system. The top ligand conformation predicted by the GOLD program was very close to the crystal structure-bound conformation. The root-mean-square deviation (RMSD) between the docked pose and its bound conformation in the crystal structure was 0.63 Å, indicating that GOLD was able to reproduce the correct pose.

As illustrated in Figure 4 a, the P6 moiety of 8 fully inserts into the binding pocket of COX-1, while the bulky secondary amide Rh6G functionality projects through the constriction site at the base of the active site and into the wide lobby in the membrane-binding domain. The position and orientation of the P6 moiety in the COX-1 active site closely resembles binding mode B previously obtained for the COX-1-selective isoxazole 3-(5-bromofuran-2-yl)-5-methyl-4-phenylisoxazole (Br-P6).^[9] In particular, the N2 isoxazole nitrogen of 8 is within hydrogen bonding distance from the *g*-OH group of Ser 530, which adopted a down position during the flexible docking simulation.^[3] The N2...O atoms are separated by 3.2 Å and display a favorable geometry for hydrogen bonding. The phenyl ring at position 4 of the isoxazole is in close contact with various hydrophobic side chains, including Leu 352, Ile 523, Tyr 355, and Phe 518. The chlorofuryl moiety is oriented toward the apex of the COX-1 active site and forms van der Waals interactions with residues Met 522, Phe 518, Leu 352, Trp 387, Tyr 385, Leu 384, and Phe 381.

The amide bond of the linker conjugating the P6 moiety makes two hydrogen bonds, one with the OH group of Tyr 355 ($d_{\text{N}\cdots\text{O}} = 2.9 \text{ Å}$) and the other with the guanidinium moiety of Arg 120 ($d_{\text{O}\cdots\text{N}} = 2.7 \text{ Å}$), which is known to play an important role in binding substrates and carboxylic acid-containing inhibitors. The linker is also engaged in hydrophobic interactions with Ile 89, Leu 93, Val 116, Val 349, Leu 359, and Leu 531. In addition, the Rh6G portion interacts with multiple hydrophobic

Table 2. COX-inhibitory activity of target compounds 7–9, 14–17, and 20.

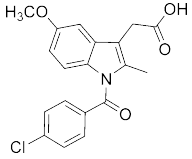
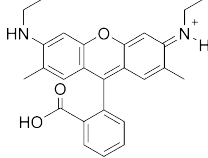
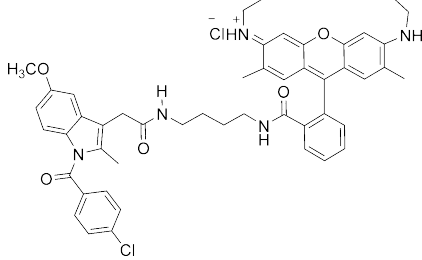
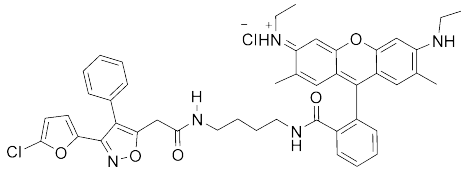
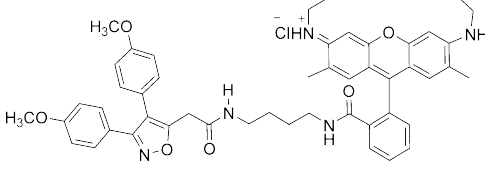
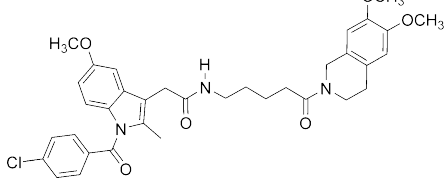
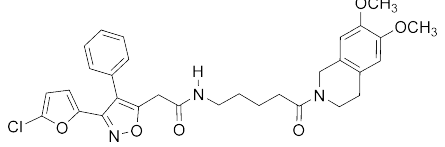
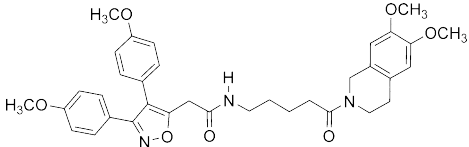
	Compound	Inhibition [%] ^[a] (IC ₅₀ [mM]) ^[b]	
		COX-1	COX-2
indomethacin		81 (0.1 0.012)	86 (4.2 0.014)
Rh6G-COOH		n.a.	n.a.
7		n.a.	28
8		69 (6.0 0.7)	n.a.
9		16	n.a.
14		n.a.	n.a.
15		23	n.a.
16		33	13

Table 2. (Continued)

Compound	Inhibition [%] ^[a] (IC ₅₀ [mm]) ^[b]	
	COX-1	COX-2
17	48	69 (0.95 0.08)
20	10	n.a.

[a] Inhibitory activity toward COX-1 and COX-2 determined at compound concentrations of 50 mm using a colorimetric COX (ovine) inhibitor screening assay kit. [b] Values are the mean SEM of three separate experiments; n.a.: not active, i.e., no inhibitory activity was observed at 50 mm.

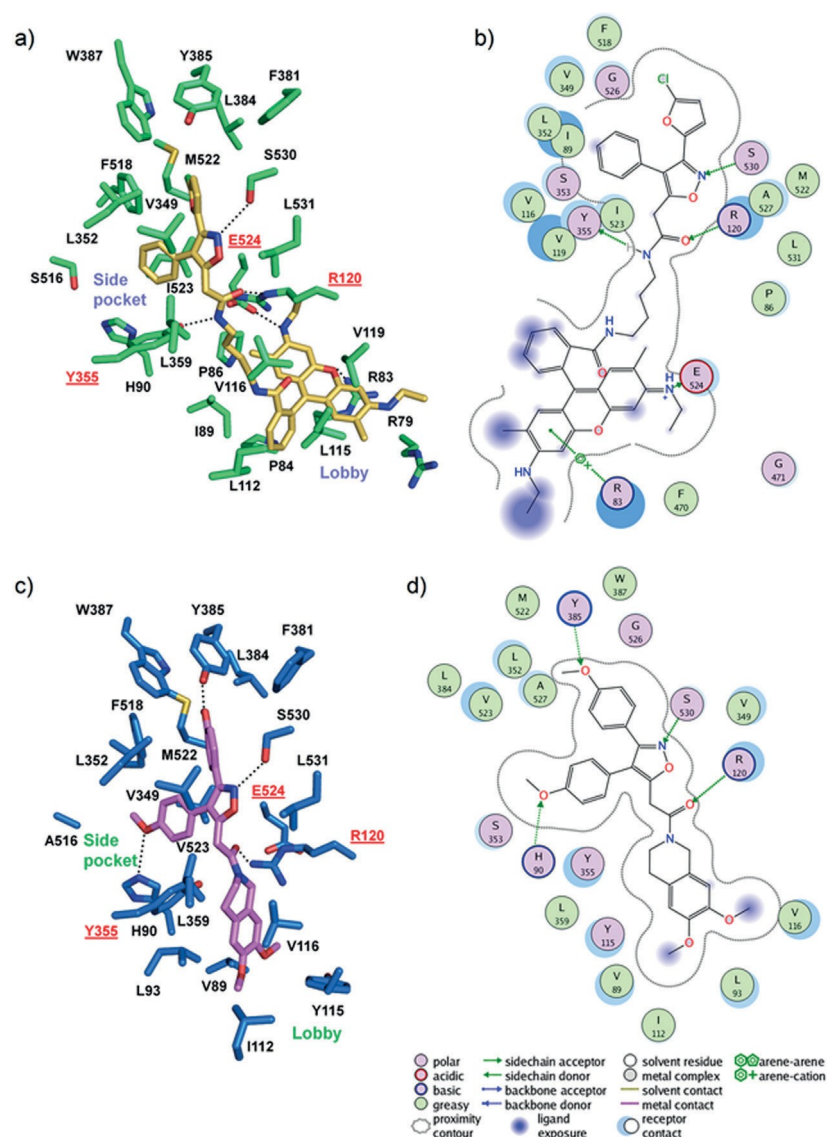


Figure 4. Binding modes of compound 8 (a, yellow) and compound 17 (c, violet) in the COX-1 and COX-2 active sites, respectively. Two-dimensional projection of b) 8–COX-1 and d) 17–COX-2 interactions generated with MOE.^[42] Only residues located within 4.5 Å of the bound ligand are displayed and labeled. Hydrogen bonds discussed in the text are depicted as dashed black lines. The constriction site residues (Arg 120, Tyr355, and Glu 524), which separate the lobby from the COX active site located above it, are underlined and colored red.

residues, including Ile 89, Pro 84, Pro 86, Leu 115, Val 119, Leu 123, and Gly 471, which provide considerable binding strength. The O2 carboxylate oxygen of Glu 524 is 2.5 Å from the positive charge on the ethyl ammonium nitrogen of the Rh6G moiety, thereby neutralizing both buried charges. The Rh6G nucleus is further anchored to the lobby region of COX-1 through a favorable cation- π interaction between its benzo-fused ring and Arg 79, as well as through an associated hydrogen bond also formed by the same amino acid residue with the central ring O1 atom of Rh6G.

Notably, in the COX-1 structure with 8 bound, although the side chain of Arg 120 reorients to form a hydrogen bond with the ligand, it is in position to preserve the salt bridge with Glu 524. In this conformation, Arg 120 no longer interacts with the OH group of Tyr 355, which in turn interacts with the ligand, leaving the bottom of the COX-1 binding site in an open conformation. Our predicted structural readjustment of Arg 120 is in agreement with that observed in the crystal structure of indomethacin-(*R*)- α -ethyl-ethanolamide complexed with COX-1, in which this residue adopts a significantly altered conformation to accommodate the ligand in comparison with crystal structures of different COX-1-ligand complexes (including NSAIDs and fatty acid substrates).^[27]

To rationalize the high inhibitory activity of compound 17 toward COX-2, docking experiments with the COX-2 binding site (PDB ID: 6COX)^[26] were also carried out. The main difference between the two COX active sites is the replacement of two isoleucine residues (Ile 434 and Ile 523) in COX-1 by two less bulky amino acids (Val 434 and Val 523) in COX-2. This double substitution opens a polar side pocket, enlarging the volume of the COX-2 active site. Additionally, the substitution of His 513 in COX-1 by Arg 513 in COX-2 allows for hydrogen bonding with the sulfonyl moiety of COX-2 inhibitors. A second difference, at the top of the channel, is the substitution of Phe 503 in COX-1 by Leu 503 in COX-2. The smaller residue in COX-2 allows Leu 384 to create an extra space at the top of the binding site in COX-2, thus permitting larger inhibitors to bind.

GOLD successfully predicted a plausible binding pose for 17 within the binding pocket of COX-2. As illustrated in Figure 4 c, the mofezolac functionality of the ligand fully inserts into the binding pocket of COX-2, while the bulky 6,7-DM-THIQ moiety projects through the constriction site at the base of the active site and into the wide lobby in the membrane-binding domain. In particular, the N2 isoxazole nitrogen of 17 is engaged in a hydrogen bond with the OH group of Ser 530 ($d_{N2\cdots O} = 2.7$ Å). The *p*-methoxyphenyl ring at position 3 of the isoxazole ring is directed toward the top of the COX-2 active site and forms hydrophobic interactions with residues Leu 352, Phe 381, Leu 384, Tyr 385, Trp 387, Phe 518, Met 522, and Gly 526. The *p*-methoxy group accepts a hydrogen bond from the Tyr 385 OH group ($d_{O\cdots O} = 3.3$ Å). Importantly, the *p*-methoxyphenyl ring at position 4 projects toward the side pocket of COX-2 and makes hydrophobic contacts with residues His 90, Tyr 355, Ala 516, Phe 518, and Val 523. The *p*-methoxy group is within hydrogen bonding distance of the nitrogen atom of the His 90 residue ($d_{O\cdots N_{H2}} = 3.2$ Å). In addition, the C=O amide of 17 forms

a hydrogen bond with the guanidinium group of Arg 120 ($d_{NH2\cdots O} = 3.0$ Å). Finally, the 6,7-DM-THIQ moiety extends into the lobby region of the enzyme and makes hydrophobic contacts with residues Val 89, Leu 93, Ile 112, Tyr 115, Val 116, Tyr 355, and Leu 359.

Comparison of the 8/COX-1 and 17/COX-2 complexes reveals striking similarities and differences in the binding of the ligands (Figure 5). Interestingly, the two inhibitors are bound in very similar conformations, with their N2 isoxazole nitrogen hydrogen bonding to Ser 530 into both isoenzymes. However, 17

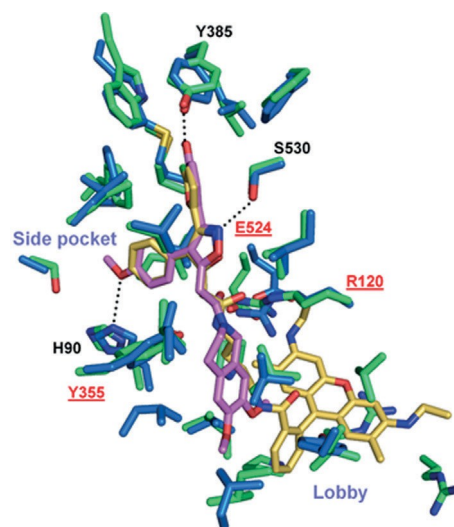


Figure 5. Superimposition of the best poses of 8 (yellow) and 17 (violet) into the COX-1 and COX-2 active sites, respectively.

makes two hydrogen bonds with the binding cleft of COX-2: one between the methoxy oxygen on the phenyl at C3 of the isoxazole and the Tyr 385 hydroxy group and the other between the methoxy oxygen on the phenyl at C4 of the isoxazole and the nitrogen atom of the His 90 imidazole ring. According to previous studies, Tyr 385 is involved in the abstraction of 13-*pro-S*-hydrogen from arachidonic acid,^[37] whereas His 90 is considered to control the access of ligands to the adjacent pocket, which is created by the replacement of Ile 523 in COX-1 by valine in the COX-2 active site and is responsible for selectivity.^[38] These hydrogen bonding interactions contribute to stabilize the binding of 17 to the COX-2 active site. Moreover, 17 shows only partial entry into the COX-1 enzyme active site, owing to the more restricted secondary internal pocket, and therefore does not exhibit significant interactions with the COX-1 active site residues. This is in agreement with the pre-dominant COX-2 inhibitory potency and selectivity of compound 17. On the other hand, the selectivity of compound 8 for COX-1 is likely to be due to the favorable interactions of the Rh6G moiety with the residues of both the constriction and lobby sites, contributing significantly to the complex stability.

Target compounds 7–9 and 15–17, each containing a P-gp-interacting fragment, were also studied for their ability to modulate efflux pump activity by measuring calcein accumula-

tion in MDCK-MDR1 cells overexpressing P-gp and by determining apparent permeability through a Caco-2 cell monolayer. Compounds 7 and 9, despite bearing the Rh6G moiety, did not interact with the efflux transporter, as demonstrated by their low EC_{50} values (Table 3). EC_{50} values were determined by fitting the percent fluorescence increase versus $\log[\text{dose}]$.^[39] All of the other compounds (8 and 15–17) showed a significant interaction with P-gp (EC_{50} values ranging from 0.42 to 4.61 μM). The permeability assay performed on the same compounds (Table 3) provided BA/AB (P_{app} , apparent permeability) values > 2 , indicating that they are P-gp substrates.^[40]

Table 3. Calcein-AM assay results and P_{app} determination.

Compound	EC_{50} [μM] ^[a]	P_{app} [nm s^{-1}] ^[b]		BA/AB
		BA	AB	
7	24 4.6	n.t.	n.t.	n.t.
8	4.61 0.7	1802	292	6.1
9	n.a.	n.t.	n.t.	n.t.
15	3.78 0.5	1283	321	3.9
16	2.80 0.1	2293	613	3.7
17	0.42 0.03	1789	442	4.0
rhodamine 6G	20	1130	484	2.3

[a] Values are the mean SEM of three separate experiments with MDCK-MDR1; n.a.: not active. [b] n.t.: not tested.

Conclusions

In this study, a set of new molecules were prepared to enable knowledge advancement of the COX active site molecular recognition, complemented by docking simulation experiments that added insight into the binding mode of these compounds. Two compounds were identified as highly selective COX-1 and COX-2 inhibitors, respectively (8, COX-1 IC_{50} = 6.0 μM ; 17, COX-2 IC_{50} = 0.95 μM). Molecular docking studies rationalized this strong COX-1 and COX-2 inhibitory activity. The diarylisoxazole moiety (P6) of 8 fully inserts into the binding pocket of COX-1, whereas the bulky Rh6G functionality projects through the constriction site into the wide lobby in the membrane-binding domain. The Rh6G portion interacts with multiple hydrophobic residues, providing considerable binding strength. On the other hand, the selective COX-2 inhibitor 17 breaches the constriction site at the mouth of the active site and projects its 6,7-DM-THIQ moiety into the sterically uncongested lobby region. Rh6G and 6,7-DM-THIQ, present in 8 and 17, respectively, were expected to confer opposite P-gp activity modulation to the two compounds. On the contrary, 8 and 17 retained COX-1 or COX-2 inhibitory activity, respectively, but both behaved as P-gp substrates (BA/AB > 2 , Table 3). All of these results have been taken into account for further studies.

Experimental Section

Chemistry

General methods: Melting points were taken on an electrothermal apparatus and are uncorrected. ^1H NMR and ^{13}C NMR spectra were

recorded on a 300 MHz Varian Mercury-VX spectrometer, and chemical shifts (δ) are reported in parts per million. Absolute values of the coupling constants are reported. FT-IR spectra were recorded on a PerkinElmer 681 spectrometer. Thin-layer chromatography (TLC) was performed on silica gel sheets with fluorescent indicator, the spots on the TLC were observed under ultraviolet light ($\lambda = 254$ or 315 nm). Column chromatography was performed using silica gel 60 with a particle size distribution of 40–63 μm and 230–400 ASTM. GC–MS analyses were performed on an HP 5995C instrument. ESI-MS analyses were performed on an Agilent 1100 LC–MSD trap system VL. All synthesized compounds were analyzed by HPLC, performed on an Agilent 1260 Infinity instrument equipped with a 1260 DAD VL + detector, and their purity was found to be higher than 95%. Indomethacin, Rh6G, 6,7-DM-THIQ, and other reagents and solvents were purchased from Sigma–Aldrich.

tert-Butyl (4-aminobutyl)carbamate (Scheme 1):^[23] Boc_2O (4.49 g, 0.0196 mol) in dioxane (80 mL) was added dropwise to a stirred solution of 1,4-diaminobutane (10.1 g, 0.115 mol) in dioxane (80 mL) at room temperature. The reaction mixture was stirred overnight at room temperature. The solvent was then evaporated under reduced pressure. H_2O (100 mL) was added, and the aqueous suspension was extracted with CH_2Cl_2 (5 \times 30 mL). The combined organic layers were dried over anhydrous sodium sulfate, and the solvent was evaporated under reduced pressure. The product was isolated as a yellow oil (3.61 g, 17 % yield): ^1H NMR (400 MHz, CDCl_3): δ = 5.14 (bs, 1H, NH: exch. with D_2O), 2.94 (q, 2H, J = 6.4 Hz, CH_2NH), 2.53 (t, 2H, J = 6.4 Hz, CH_2NH_2), 1.36–1.26 (m, 13H, $\text{CH}_2(\text{CH}_2)_2\text{CH}_2$ and $\text{C}(\text{CH}_3)_3$), 1.07 ppm (s, 2H, NH_2 : exchange with D_2O); FT-IR (neat): $\tilde{\nu}$ = 3359, 2976, 2933, 2866, 1694, 1528, 1453, 1391, 1365, 1276, 1252, 1174, 1042, 989, 867, 781 cm^{-1} .

N-[9-(2-Carboxyphenyl)-6-(ethylamino)-2,7-dimethyl-3H-xanthen-3-ylidene]ethanaminium (Rh6G-COOH) (Scheme 2):^[24] A solution of NaOH (75.6 mg, 1.89 mmol) in H_2O (60 mL) was added to a stirred solution of Rh6G (500 mg, 1.04 mmol) in absolute EtOH (50 mL) at room temperature. The reaction mixture was stirred at reflux overnight. The EtOH was then evaporated under reduced pressure, and 37 % HCl was added until an acidic pH was achieved. The product was isolated after filtration as a pink solid (258 mg, 55 % yield); mp: > 300 $^{\circ}\text{C}$. ^1H NMR (300 MHz, $[\text{D}_6]\text{acetone}$): δ = 8.41 (bs, 1H, NH^+ : exch. with D_2O), 7.91 (d, 1H, J = 7.6 Hz, arom.), 7.75–7.59 (m, 2H, arom.), 7.17 (d, 1H, J = 7.6 Hz, arom.), 6.36 (s, 2H, arom.), 6.33 (s, 2H, arom.), 4.67 (bs, 1H, NH: exch. with D_2O), 3.24 (q, 4H, J = 7.2 Hz, 2 NCH_2CH_3), 2.90 (bs, 1H, COOH: exch. with D_2O), 1.93 (s, 6H, 2 ArCH_3), 1.27 ppm (t, 6H, J = 7.2 Hz, 2 NCH_2CH_3); FT-IR (KBr): $\tilde{\nu}$ = 3415, 2924, 1608, 1530, 1501, 1365, 1307, 1187, 1016, 793 cm^{-1} ; ESI-MS (m/z): $\text{C}_{26}\text{H}_{27}\text{N}_2\text{O}_3$, 415 [M] $^+$, 437 [M + Na] $^+$.

tert-Butyl-(4-{2-[1-(4-chlorobenzoyl)-5-methoxy-2-methyl-1H-indol-3-yl]acetamido}butyl)carbamate (1): *tert*-Butyl (4-aminobutyl)carbamate (320 mg, 1.7 mmol), HOBt (151 mg, 0.81 mmol), DIEA (225 mg, 1.7 mmol), and EDC-HCl (153 mg, 0.798 mmol) were added to nitrogen-flushed, three-necked flask equipped with a magnetic stirrer, nitrogen inlet, and two dropping funnels, containing a solution of indomethacin (210 mg, 0.588 mmol) solubilized in DMF (14 mL). The mixture was stirred at room temperature for 48 h. Then, H_2O (20 mL) was added, and the aqueous solution was extracted with EtOAc (3 \times 30 mL). The combined organic layers were washed with brine and dried over anhydrous sodium sulfate, and the solvent was evaporated under reduced pressure. Column chromatography of the crude residue on silica gel using $\text{CHCl}_3/\text{MeOH}$ (95:5) as a mobile phase afforded the target compound as a yellow solid (140 mg, 45 % yield). ^1H NMR (300 MHz, CDCl_3): δ =

7.67 (d, 2H, $J=8.4$ Hz, arom.), 7.49 (d, 2H, $J=8.4$ Hz, arom.), 6.90–6.85 (m, 2H, arom.), 6.71–6.68 (m, 1H, arom.), 5.78 (bs, 1H, CONHCH_2 : exch. with D_2O), 4.58 (bs, 1H, NHCOO : exch. with D_2O), 3.82 (s, 3H, OCH_3), 3.63 (s, 2H, ArCH_2CONH), 3.25–3.18 (m, 2H, $\text{NHCH}_2(\text{CH}_2)_3$), 3.15–2.98 (m, 2H, $(\text{CH}_2)_3\text{CH}_2\text{NH}$), 2.39 (s, 3H, ArCH_3), 1.50–1.37 ppm [m, 13H, CH_2CH_2 and $\text{C}(\text{CH}_3)_3$].

tert-Butyl (4-{2-[3-(5-chlorofuran-2-yl)-4-phenylisoxazol-5-yl]-acetamido}butyl)carbamate (2): Compound 2 was prepared using the same procedure used to synthesize 1, replacing indomethacin with P6-COOH to give a yellow solid (116.8 mg, 42 % yield); mp: 126.5–127.8°C; ^1H NMR (300 MHz, CDCl_3): d = 7.48–7.44 (m, 3H,

arom.), 7.38–7.35 (m, 2H arom.), 6.30 (d, 1H, $J=3.5$ Hz, furyl), 6.16 (d, 1H, $J=3.5$ Hz, furyl), 6.04 (bs, 1H, CONHCH_2 : exch. with D_2O), 4.58 (s, 1H, NHBOc : exch. with D_2O), 3.66 (s, 2H, isoxazole- CH_2CO), 3.27 (q, 2H, $J=6.8$ Hz, CONHCH_2), 3.18–3.10 (m, 2H, CH_2NHCO), 1.54–1.48 (m, 4H, CH_2CH_2), 1.44 ppm (s, 9H, $\text{C}(\text{CH}_3)_3$); ^{13}C NMR (75 MHz, CDCl_3): d = 166.1, 130.2, 129.1, 129.06, 114.4, 108.2, 59.7, 39.9, 38.3, 34.0, 32.1, 31.4, 31.1, 29.9, 29.5, 28.6, 27.8, 22.9, 14.3 ppm; FT-IR (KBr): $\tilde{\nu}$ = 3346, 2941, 1683, 1658, 1539, 1521, 1437, 1366, 1261, 1172, 1019, 941, 892, 787, 699 cm^{-1} ; ESI-MS (m/z): $\text{C}_{24}\text{H}_{28}\text{ClN}_3\text{O}_5$, 496 $[M+\text{Na}]^+$.

tert-Butyl (4-{2-[3,4-bis(4-methoxyphenyl)isoxazol-5-yl]acetamido}butyl)carbamate (3). *tert-Butyl (4-aminobutyl)carbamate* (478 mg, 2.54 mmol), HOBt (185 mg, 1.21 mmol), dry DIEA (328 mg,

2.54 mmol), and EDC-HCl (229 mg, 1.19 mmol) were added to a so-

lution of mofezolac (300 mg, 0.88 mmol) solubilized in dry DMF (15 mL) in a nitrogen-flushed, three-necked flask equipped with a magnetic stirrer, nitrogen inlet, and two dropping funnels. The

mixture was stirred at room temperature for 48 h. Then, H_2O (20 mL) was added, and the aqueous solution was extracted with EtOAc (3 \times 30 mL). The combined organic layers were washed with

brine and dried over anhydrous sodium sulfate, and the solvent was evaporated under vacuum. The product was isolated as a yellow solid (184 mg, 41 % yield) by column chromatography (silica gel, $\text{CHCl}_3/\text{MeOH}$ = 95:5). ^1H NMR (300 MHz, CDCl_3): d = 7.38

(d, 2H, $J=8.9$ Hz, arom.), 7.16 (d, 2H, $J=8.8$ Hz, arom.), 6.90 (d, 2H, $J=8.8$ Hz, arom.), 6.84 (d, 2H, $J=8.9$ Hz, arom.), 6.09 (bs, 1H, NH : exch. with D_2O), 4.60 (bs, 1H, NH : exch. with D_2O), 3.83 (s, 3H,

OCH₃), 3.80 (s, 3H, OCH₃), 3.68 (s, 2H, ArCH_2CON), 3.28 (q, 2H $J=6.3$ Hz, NHCH_2), 3.15–3.05 (m, 2H, CH_2NH), 1.54–1.37 ppm [m, 13H, CH_2CH_2 and $\text{C}(\text{CH}_3)_3$]; ^{13}C NMR (75 MHz, CDCl_3): d = 166.8, 162.9,

161.4, 160.8, 159.7, 156.3, 131.3, 130.0, 121.6, 121.2, 117.7, 114.6, 114.2, 79.5, 55.6, 55.4, 40.2, 39.9, 34.4, 29.9, 28.6, 27.8, 27.6, 26.7 ppm; ESI-MS (m/z): $\text{C}_{28}\text{H}_{35}\text{N}_3\text{O}_6$, 532 $[M+\text{Na}]^+$.

4-{2-[1-(4-Chlorobenzoyl)-5-methoxy-2-methyl-1H-indol-3-yl]acetamido}butan-1-aminium chloride (4): Dry HCl (obtained by dripping conc. H_2SO_4 into 37 % HCl and NaCl) was bubbled in a solution

of *tert*-butyl-(4-{2-[1-(4-chlorobenzoyl)-5-methoxy-2-methyl-1H-indol-3-yl]acetamido}butyl)carbamate (1; 140 mg, 0.265 mmol) in dry CH_2Cl_2 (10 mL) at 0°C (ice bath). After 3 h, the solvent of the brown suspension was evaporated under reduced pressure, and the product was isolated as a brown solid (118 mg, 96 % yield). ^1H NMR (400 MHz, $[\text{D}_6]\text{DMSO}$): d = 8.20–8.11 (bs, 1H, NH : exch. with D_2O), 8.00–7.80 (bs, 3H, NH_3^+ : exchange with D_2O), 7.66–7.58 (m, 4H, arom.), 7.10 (d, 1H, $J=2.2$ Hz, arom.), 6.88 (d, 1H, $J=9.2$ Hz,

4-{2-[3-(5-chlorofuran-2-yl)-4-phenylisoxazol-5-yl]acetamido}butyl)-carbamate (2) as a reagent to give a yellow oil (98.8 mg, quantitative yield); ^1H NMR (300 MHz, $[\text{D}_6]\text{DMSO}$): d = 8.50–8.40 (m, 1H, CONHCH_2 : exch. with D_2O), 8.14 (bs, 3H, NH_3^+ : exchange with D_2O), 7.46–7.38 (m, 2H, arom.), 7.36–7.30 (m, 3H, arom.), 6.54 (d, 1H, $J=3.5$ Hz, furyl), 6.38 (d, 1H, $J=3.5$ Hz, furyl), 3.61 (s, 2H, CH_2CO), 3.20–2.96 (m, 2H, CH_2NH_3^+), 2.74–2.64 (m, 2H, CONHCH_2), 1.54–1.36 ppm (m, 4H, CH_2CH_2); ^{13}C NMR (75 MHz, $[\text{D}_6]\text{DMSO}$): d = 166.6, 165.9, 165.4, 152.4, 143.6, 137.6, 130.4, 130.2, 129.4, 129.2, 128.9, 116.8, 114.8, 109.5, 94.6, 70.4, 63.5, 38.9, 33.2, 26.5, 25.0 ppm; FT-IR (KBr): $\tilde{\nu}$ = 3405, 1633, 1266, 1134, 1017, 793 cm^{-1} ; ESI-MS (m/z): $\text{C}_{24}\text{H}_{28}\text{ClN}_3\text{O}_5$, 496 $[M+\text{H}]^+$, (37) $\text{C}_{24}\text{H}_{27}\text{ClN}_3\text{O}_5$, 495 $[M+\text{H}]^+$, (100).

N-(4-Aminobutyl)-2-(3,4-bis(4-methoxyphenyl)isoxazol-5-yl)acetamide hydrochloride (6): Dry HCl (obtained by dripping H_2SO_4 conc. in 37 % HCl and NaCl) was bubbled in a solution of *tert*-butyl (4-{2-[3,4-bis(4-methoxyphenyl)isoxazol-5-yl]acetamido}butyl)-carbamate (3) (170 mg, 0.33 mmol) in dry CH_2Cl_2 (15 mL). After 2 h, the reaction mixture became a suspension. The solvent was then evaporated under vacuum, and the product was isolated as a brown solid (quantitative yield) and was used without any further purification. ^1H NMR (300 MHz, CDCl_3): d = 7.35 (d, 2H, $J=8.8$ Hz, arom.), 7.15 (d, 2H, $J=8.8$ Hz, arom.), 6.88 (d, 2H, $J=8.8$ Hz, arom.), 6.81 (d, 2H, $J=8.8$ Hz, arom.), 6.80–6.74 (bs, 1H, NH : exch. with D_2O), 3.80 (s, 3H, OCH₃), 3.77 (s, 3H, OCH₃), 3.64 (s, 2H, ArCH_2CON),

3.25 (q, 2H, $J=6.1$ Hz, NHCH_2), 2.71 (t, 2H, $J=6.6$ Hz, CH_2NH_2), 2.05–1.95 (bs, 2H, NH_2 : exchange with D_2O), 1.57–1.43 ppm (m, 4H, CH_2CH_2); ^{13}C NMR (75 MHz, CDCl_3): d = 166.9, 163.2, 161.3, 160.8, 159.6, 131.30, 131.27, 130.0, 129.9, 121.6, 121.2, 117.7, 114.5, 114.2,

55.5, 55.4, 41.7, 40.0, 34.3, 30.8, 27.1 ppm; ESI-MS (m/z): $\text{C}_{23}\text{H}_{27}\text{N}_3\text{O}_4$, 410 $[M+\text{H}]^+$.

N-(9-(2-((4-{2-[1-(4-Chlorobenzoyl)-5-methoxy-2-methylindolin-3-yl]acetamido}butyl)carbamoyl)phenyl-6-(ethylamino)-2,7-dimethyl-3H-xanthen-3-ylidene)ethanaminium chloride (7): Bbenzotriazol-1-yl-oxytripyrrolidinophosphonium hexafluorophosphate (PyBOP; 20.2 mg, 0.039 mmol) and triethylamine (50.3 mg, 0.39 mmol) were added to a stirred solution of Rh6G-COOH (N-[9-

(2-carboxyphenyl)-6-(ethylamino)-2,7-dimethyl-3H-xanthen-3-ylidene)ethanaminium chloride (18 mg, 0.037 mmol) in $\text{CHCl}_3/\text{DMSO}$

(3:1, 4 mL). After 2 h, a solution of 4-{2-[1-(4-chlorobenzoyl)-5-methoxy-2-methyl-1H-indol-3-yl]acetamido}butan-1-aminium chloride (4) in $\text{CHCl}_3/\text{DMSO}$ (3:2) (5 mL) was added dropwise, and the mixture was stirred for 24 h at room temperature. The solvent was then removed under reduced pressure. Column chromatography of the crude residue on silica gel using hexane/EtOAc (1:1) as the mobile phase afforded the target compound as a yellow semi-solid (15 mg, 47 % yield): ^1H NMR (300 MHz, CDCl_3): d = 8.52–8.30 (bs,

3H, $2\text{NHCO} + \text{NH}^+$, exchange with D_2O), 7.87–7.85 (m, 1H, arom.), 6.66 (dd, 1H, $J=9.2$ and 2.2 Hz, arom.), 3.72 (s, 3H, OCH₃), 3.46 (s, 2H, ArCH_2CON), 3.06–2.97 (m, 2H, CH_2NH_3^+), 2.78–2.66 (m, 2H, NHCH_2), 2.20 (s, 3H, ArCH_3), 1.60–1.19 ppm (m, 4H, CH_2CH_2).

N-(4-Aminobutyl)-2-[3-(5-chlorofuran-2-yl)-4-phenylisoxazol-5-yl]acetamide hydrochloride (5): Compound 5 was prepared following the same procedure used for compound 4 using *tert*-butyl

7.69–7.67 (m, 2H, arom.), 7.49–7.46 (m, 2H, arom.), 7.45–7.43 (m, 1H, arom.), 7.05–7.02 (m, 1H, arom.), 6.92 (d, 1H, $J = 2.4$ Hz, arom.), 6.87 (d, 1H, $J = 9.2$ Hz, arom.), 6.66 (dd, 1H, $J = 9.2$ and 2.4 Hz, arom.), 6.34 (s, 2H, arom.), 6.25–6.23 (bs, 1H, NH: exch. with D₂O), 6.18 (s, 2H, arom.), 3.78 (s, 3H, OCH₃), 3.60 (s, 2H, ArCH₂CO), 3.21 (q, 4H, $J = 7.2$ Hz, 2 NHCH₂CH₃), 3.05 (m, 4H, CH₂(CH₂)₂CH₂), 2.38 (s, 3H, CH₃), 1.88 (s, 6H, 2 CH₃), 1.32 (t, 6H, $J = 7.2$ Hz, NHCH₂CH₃), 1.29–1.20 ppm (m, 4H, CH₂(CH₂)₂CH₂); ¹³C NMR (100 MHz, CDCl₃):

δ = 170.1, 168.5, 156.4, 151.9, 147.6, 139.5, 136.4, 134.1, 132.6, 131.4, 131.1, 130.8, 129.3, 128.63, 128.2, 124.0, 122.8, 118.0, 115.2, 113.5, 112.3, 110.9, 106.2, 101.2, 96.7, 94.6, 65.2, 60.6, 55.9, 39.5, 39.4, 38.6, 32.4, 31.4, 29.9, 26.1, 25.9, 21.2, 16.8, 14.9, 14.4, 13.6 ppm; FT-IR (neat): $\tilde{\nu}$ = 3429, 3330, 3051, 2963, 2923, 2854, 1675, 1621, 1517, 1468, 1322, 1262, 1218, 1149, 1090, 1016, 925,

879, 801, 743, 693 cm^{-1} ; ESI-MS (m/z): $\text{C}_{49}\text{H}_{50}^{35}\text{ClN}_5\text{O}_5$, 824 [$M+H$]⁺ (38), $\text{C}_{49}\text{H}_{50}^{35}\text{ClN}_5\text{O}_5$, 824 [$M+H$]⁺ (100).

N-(9-[2-[(4-[2-[3-(5-Chlorofuran-2-yl)-4-phenylisoxazol-5-yl]acetamido)butyl]carbamoyl]phenyl]-6-(ethylamino)-2,7-dimethyl-3*H*-xanthen-3-ylidene)ethanaminium chloride (8): EDC·HCl (30 mg, 0.158 mmol), HOBt (31.5 mg, 0.206 mmol), DIEA (114 mg, 0.735 mmol), and compound 5 (60 mg, 0.147 mmol) were added to a stirred solution of *N*-(9-(2-carboxyphenyl)-6-(ethylamino)-2,7-dimethyl-3*H*-xanthen-3-ylidene)ethanaminium (77 mg, 0.158 mmol) in DMF (6 mL). The reaction mixture was stirred overnight at room temperature. The solvent was then removed under reduced pressure. Column chromatography of the crude residue on silica gel using hexane/EtOAc (1:1), followed by $\text{CHCl}_3/\text{MeOH}$ (95:5), as the mobile phase afforded the target compound as a brown oil (18 mg, 15% yield): ^1H NMR (300 MHz, CDCl_3): δ = 7.99–7.97 (bs, 1H, NH^+ : exch. with D_2O), 7.82–7.79 (m, 1H, arom.), 7.43–7.35 (m, 7H, arom.), 7.04–6.96 (m, 1H, arom.), 6.72–6.64 (bs like triplet, 1H, CONHCH_2 : exch. with D_2O), 6.31 (s, 2H, arom.), 6.22 (d, 1H, J = 2.8 Hz, furanyl), 6.18 (s, 2H, arom.), 6.10 (d, 1H, J = 2.8 Hz, furanyl), 3.61 (s, 2H, CH_2CO), 3.60–3.40 (bs, 2H, 2 NHCH_2CH_3 : exchange with D_2O), 3.17 (q, 4H, J = 7.1 Hz, 2 NHCH_2CH_3), 3.10–3.04 (m, 4H, $\text{CH}_2(\text{CH}_2)_2\text{CH}_2$), 1.87 (s, 6H, 2 ArCH_3), 1.30–1.22 ppm (m, 10H, 2 NHCH_2CH_3 and $(\text{CH}_2)_2\text{CH}_2\text{CH}_2$ and $\text{CH}_2\text{CH}_2(\text{CH}_2)_2$); ^{13}C NMR (100 MHz, CDCl_3): δ = 168.5, 166.0, 163.7, 162.5, 153.6, 152.4, 151.6, 147.4, 143.3, 138.5, 132.4, 131.0, 130.0, 128.8, 128.6, 128.57, 128.47, 128.0, 123.7, 122.6, 117.9, 116.9, 113.9, 107.9, 106.0, 96.5, 65.1, 39.6, 39.2, 38.3, 33.5, 29.7, 25.9, 25.2, 16.6, 14.7 ppm; ESI-MS (m/z): $\text{C}_{45}\text{H}_{44}^{37}\text{ClN}_5\text{O}_5$, 792 [$M+H$]⁺ (39), $\text{C}_{45}\text{H}_{44}^{35}\text{ClN}_5\text{O}_5$, 792 [$M+H$]⁺ (100).

N-(9-[2-[(4-[2-[3,4-Bis(4-methoxyphenyl)isoxazol-5-yl]acetamido)-butyl]carbamoyl]phenyl]-6-(ethylamino)-2,7-dimethyl-3*H*-xanthen-3-ylidene)ethanaminium chloride *N*-(4-[2-[3,4-bis(4-methoxyphenyl)isoxazol-5-yl]acetamido)butyl]-2-[6-(ethylamino)-3-(ethylimino)-2,7-dimethyl-3*H*-xanthen-9-yl]benzamide (9): PyBOP (338 mg, 0.650 mmol) and triethylamine (379 mg, 3.75 mmol, 0.052 mL) were added to a stirred solution of (Z)-2-(6-(ethylamino)-3-(ethylimino)-2,7-dimethyl-3*H*-xanthen-9-yl)benzoic acid (146 mg, 0.03 mmol) in $\text{CH}_2\text{Cl}_2/\text{DMSO}$ (3:1, 22 mL) at 0 $^\circ\text{C}$ (ice bath). After 2 h stirring at 0 $^\circ\text{C}$, a solution of compound 6 (133 mg, 0.3 mmol) in $\text{CH}_2\text{Cl}_2/\text{DMSO}$ (3:2, 22 mL) was added dropwise, and the reaction mixture was stirred for 24 h at room temperature. The solvent was then removed under reduced pressure. Column chromatography of the crude residue on silica gel using hexane/EtOAc (1:1) as the mobile phase afforded the target compound as a brown oil (21.7 mg, 90% yield): ^1H NMR (300 MHz, CDCl_3): δ = 7.90–7.84 (m, 1H, arom.), 7.46–7.41 (m, 2H, arom.), 7.39–7.32 (m, 2H, arom.), 7.22–7.16 (m, 2H, arom.), 7.07–7.01 (m, 1H, arom.), 6.90–6.80 (m, 3H, arom.), 6.45–6.30 (bs, 2H, 2 NH : exchange with D_2O), 6.34 (s, 2H, arom.), 6.21 (s, 2H, arom.), 3.80 (s, 3H, OCH_3), 3.79 (s, 3H, OCH_3), 3.62 (s, 2H, ArCH_2NCO), 3.52 (bs, 2H, 2 NHCH_2CH_3 : exchange with D_2O), 3.23–3.05 (m, 8H, 2 NHCH_2CH_3 and $\text{CH}_2(\text{CH}_2)_2\text{CH}_2$), 1.89 (s, 6H, 2 ArCH_3), 1.37–1.24 [m, 8H, 2 NHCH_2CH_3 and $(\text{CH}_2)_2\text{CH}_2\text{CH}_2$], 1.14–1.05 ppm (m, 2H, $\text{CH}_2\text{CH}_2(\text{CH}_2)_2$); ^{13}C NMR (75 MHz, CDCl_3): δ = 168.7, 166.8, 163.2, 161.2, 160.7, 159.6, 153.8, 151.9, 147.6, 132.7, 131.4, 130.0, 128.8, 128.7, 128.3, 124.0, 122.9, 121.9, 121.5, 118.1, 117.7, 114.5, 114.1, 106.3, 96.8, 96.7, 65.3, 55.5, 55.4, 42.9, 39.9, 39.6, 34.2, 26.0, 25.8, 16.9, 14.9 ppm; FT-IR (neat): $\tilde{\nu}$ = 3429, 3330, 3051, 2963, 2923, 2854, 1675, 1621, 1517, 1468, 1322, 1262, 1218, 1149, 1090, 1016, 925, 879, 801, 743, 693 cm^{-1} ; ESI-MS (m/z): $\text{C}_{49}\text{H}_{51}\text{N}_5\text{O}_6$, 828 [$M+Na$]⁺.

5-[(*tert*-Butoxycarbonyl)amino]pentanoic acid (10): NaHCO_3 (1.44 g, 0.017 mmol) and Boc_2O (2.8 g, 0.013 mol) in dioxane (10 mL) were added to a solution of 5-aminovaleric acid (1.0 g,

9 mmol) in H_2O (25 mL) at 0 $^\circ\text{C}$. The mixture was stirred overnight at room temperature. The reaction mixture was then acidified with 3 N HCl and extracted with EtOAc. The combined organic layers were dried over anhydrous sodium sulfate, and the solvent was evaporated under reduced pressure to afford the crude solid, which was recrystallized by $\text{CHCl}_3/\text{hexane}$. The pure compound was obtained as a white solid (2.1 g, 97%): mp: 53–56 $^\circ\text{C}$ (lit. mp: 45–48 $^\circ\text{C}$); 25 ^1H NMR (300 MHz, CDCl_3): δ = 4.56 (bs 1H, NH : exch. with D_2O), 3.10–3.05 (m, 2H, CH_2NH), 2.34 (t, 2H, J = 7.2 Hz, CH_2CO), 1.66–1.59 (m, 2H, $\text{CH}_2\text{CH}_2\text{CO}$), 1.54–1.46 (m, 2H, $\text{CH}_2\text{CH}_2\text{CH}_2\text{CO}$), 1.40 ppm (s, 9H, $t\text{Bu}$); ^{13}C NMR (75 MHz, CDCl_3): δ = 179.0, 156.3, 79.5, 40.3, 33.8, 29.6, 28.6, 22.1 ppm; ESI-MS (m/z): $\text{C}_{10}\text{H}_{19}\text{NO}_4$, 240 [$M+Na$]⁺.

tert-Butyl {5-[6,7-dimethoxy-3,4-dihydroisoquinolin-2-(1*H*)-yl]-5-oxopentyl}carbamate (12): EDC·HCl (0.42 g, 2.20 mmol), HOBt (1.26 g, 9.33 mmol), drained DIPEA (0.061 mL, 3.60 mmol), and 5-[(*tert*-butoxycarbonyl)amino]pentanoic acid (10) (0.385 g, 1.77 mmol) were added at room temperature to a solution of 6,7-DMTIQ (11) (1.3 g, 6.73 mmol) in dry DMF (10 mL). The mixture was stirred overnight, then NaHCO_3 and brine were added, and the aqueous phase was extracted with EtOAc. The combined organic layers were dried over anhydrous sodium sulfate, and the solvent was evaporated under reduced pressure to afford a brown oil. Column chromatography of the crude reaction mixture on silica gel using EtOAc/MeOH (9:1) as the mobile phase to give the target compound as a yellow oil (160 mg, 23% yield): ^1H NMR (300 MHz, CDCl_3): δ = 6.60–6.57 (m, 2H, arom.), 4.70 (s, 1H, NH : exch. with D_2O), 4.63 (s, slightly broad, 1H, ArCHHNCO , conformer signal), 4.52 (s, slightly broad, 1H, ArCHHNCO , conformer signal), 3.84–3.82 (m, 6H, 2 OCH_3 , conformers signals), 3.79 (t, 1H, J = 5.9 Hz, $\text{ArCH}_2\text{CHHNCO}$, conformer signal), 3.64 (t, 1H, J = 5.9 Hz, $\text{ArCH}_2\text{CHHNCO}$, conformer signal), 3.12 (q, 2H, J = 7.0 Hz, NHCH_2), 2.79 (t, 1H, J = 5.9 Hz, $\text{ArCHHCH}_2\text{NCO}$, conformer signal), 2.73 (t, 1H, J = 5.9 Hz, $\text{ArCHHCH}_2\text{NCO}$, conformer signal), 2.40 (t, 2H, J = 7.0 Hz, $(\text{CH}_2)_3\text{CH}_2\text{CON}$), 1.73–1.63 (m, 2H, $\text{CH}_2\text{CH}_2\text{CO}$), 1.57–1.48 (m, 2H, $(\text{CH}_2)_2\text{CH}_2\text{CH}_2\text{NH}$), 1.41 ppm (s, 9H, $t\text{Bu}$); ^{13}C NMR (75 MHz, CDCl_3): δ = 171.9, 156.3, 148.1, 148.0, 125.9, 125.6, 111.4, 109.6, 79.2, 56.1, 47.2, 44.1, 40.3, 33.8, 29.9, 28.6, 28.2, 22.4 ppm; FT-IR (neat): $\tilde{\nu}$ = 3348, 2936, 1694, 1518, 1453, 1366, 1272, 1166, 1116, 1037, 754 cm^{-1} ; ESI-MS (m/z): $\text{C}_{21}\text{H}_{32}\text{N}_2\text{O}_5$, 415 [$M+Na$]⁺.

5-Amino-1-[6,7-dimethoxy-3,4-dihydroisoquinolin-2-(1*H*)-yl]pentan-1-one hydrochloride (13): Dry HCl (obtained by dripping H_2SO_4 conc. into 37% HCl and NaCl) was bubbled into a solution of 12 (600 mg, 1.53 mmol) in dry CH_2Cl_2 (10 mL). The solvent was evaporated under reduced pressure to afford the crude solid, which was recrystallized by $\text{CHCl}_3/\text{hexane}$. The pure compound was obtained as a yellow solid (451 mg; 90% yield). ^1H NMR (300 MHz, CDCl_3): δ = 8.15–8.07 (bs, 3H, NH_3^+ : exchange with D_2O), 6.76 (slightly broad singlet, 1H, arom.), 6.71 (slightly broad singlet, 1H, arom.), 4.53 (slightly broad singlet, 1H, ArCHHNCO , conformer signal), 4.48 (slightly broad singlet, 1H, ArCHHNCO , conformer signal), 3.70–3.68 (m, 6H, 2 OCH_3 , conformer signal), 3.65–3.60 (m, 2H, $\text{ArCH}_2\text{CH}_2\text{NCO}$), 2.82–2.68 (m, 3H, CH_2NH_3^+ and $\text{ArCHHCH}_2\text{NCO}$), 2.65–2.60 (m, 1H, $\text{ArCHHCH}_2\text{NCO}$), 2.49–2.38 (m, 2H, CH_2CON), 1.65–1.48 ppm (m, 4H, $(\text{CH}_2)_2\text{CH}_2\text{NH}_3^+$); FT-IR (KBr): $\tilde{\nu}$ = 3405, 2938, 2254, 1618, 1518, 1466, 1369, 1257, 1216, 1113, 912, 738, 669 cm^{-1} .

2-[1-(4-Chlorobenzoyl)-5-methoxy-2-methyl-1*H*-indol-3-yl]-*N*-(5-[6,7-dimethoxy-3,4-dihydroisoquinolin-2-(1*H*)-yl]-5-oxopentyl)acetamide (14): Compound 13 (164 mg, 0.5 mmol), HOBt (104 mg, 0.77 mmol), EDC·HCl (112 mg, 0.58 mmol), and dry DIPEA (0.17 mL, 0.97 mmol) were added to a stirred solution of 2-[1-(4-chloroben-

zoyl)-5-methoxy-2-methylindolin-3-yl]acetic acid (indomethacin; 300 mg, 0.84 mmol) in dry DMF (10 mL) under argon atmosphere at room temperature. The resulting yellow reaction mixture was stirred overnight. Then, saturated aq. NaHCO₃ (100 mL) was added, and the aqueous solution was extracted with EtOAc (3 x 30 mL). The combined organic layers were washed with brine and dried over anhydrous sodium sulfate, and the solvent was evaporated under reduced pressure. Column chromatography of the crude residue on silica gel using CHCl₃/MeOH (15:1) as the mobile phase afforded the target compound as an oil (278 mg, 50 % yield): ¹H NMR (300 MHz, CDCl₃): δ = 7.71–7.62 (m, 2H, arom.), 7.50–7.39 (m, 2H, arom.) 6.90–6.82 (m, 2H, arom.), 6.67–6.56 (m, 3H, arom.), 6.23–6.09 (two broad triplets, 1 H, NH: exch. with D₂O, two conformers signals), 4.52 (slightly broad singlet, 1 H, ArCHHNCO, conformer signal), 4.48 (slightly broad singlet, 1 H, ArCHHNCO, conformer signal), 3.84–3.81 (m, 6 H, 2 OCH₃, conformers signals), 3.78 (s, 3 H, OCH₃), 3.73 (t, 1 H, J = 5.9 Hz, ArCH₂CHHNCO, conformer signal), 3.64–3.54 (m, 3H, CH CONH and ArCH CHHNCO, conformers sig-

nals), 3.21 (q, 2H, J = 6.24 Hz, NHCH₂(CH₂)₃, conformer signal), 2.76 (t, 1H, J = 5.7 Hz, ArCHHCH₂NCO, conformer signal), 2.69 (t, 1H, J = 5.7 Hz, ArCHHCH₂NCO, conformer signal), 2.40–2.28 (m, 5H, CH

and CH₂CO-isoquinoline), 1.62–1.42 ppm (m, 4H, NHCH₂(CH₂)₂CH₂); ¹³C NMR (75 MHz, CDCl₃, conformers signals): δ = 171.6, 170.26, 170.23, 168.6, 156.4, 148.15, 148.06, 147.91, 147.87, 139.63, 139.56, 136.6, 136.5, 133.9, 131.4, 131.2, 130.73, 130.69, 129.3, 127.1, 125.8, 125.5, 124.3, 115.3, 113.2, 112.4, 111.8, 111.7, 111.4, 111.3, 109.6, 109.5, 109.0, 101.0, 56.27, 56.21, 56.12, 56.0, 55.9, 47.1, 44.0, 43.4, 39.9, 39.2, 33.0, 32.6, 32.5, 29.9, 29.2, 28.2, 21.86, 21.81, 13.6 ppm; FT-IR (KBr): $\tilde{\nu}$ = 3306, 3069, 2930, 2835, 1675, 1645, 1518, 1477, 1455, 1358, 1323, 1257, 1223, 1148, 1115, 1088, 1064, 1034, 1014, 925, 851, 832, 754 cm⁻¹; ESI-MS (*m/z*): C₃₅H₃₈³⁷ClN₃O₆ 654 [*M* + H]⁺ (33), C₃₅H₃₈³⁵ClN₃O₆ 654 [*M* + H]⁺ (100).

2-[3-(5-Chlorofuran-2-yl)-4-phenylisoxazol-5-yl]-N-[5-(3,4-dihydro-6,7-dimethoxyisoquinolin-2-(1*H*)-yl)]-5-oxopentylacetamide (15): Compound 13 (26 mg, 0.08 mmol), HOBT (16 mg, 0.12 mmol), EDC·HCl (18 mg, 0.09 mmol), and dry DIPEA (0.023 mL, 0.135 mmol) were added to a solution of 2-[3-(5-chlorofuran-2-yl)-4-phenylisoxazol-5-yl]acetic acid (P6-COOH; 41 mg, 0.14 mmol) in dry DMF (3 mL) at room temperature. The reaction mixture was stirred for 24 h, then H₂O (20 mL) was added, and the aqueous solution was extracted with EtOAc (3 x 30 mL). The combined organic layers were washed with brine and dried over anhydrous sodium sulfate, and the solvent was evaporated under reduced pressure. The crude residue was purified by column chromatography on a silica gel column with EtOAc as the mobile phase to give the target compound as a yellow solid (16.2 mg, 35 % yield): mp: 225–228 °C; ¹H NMR (300 MHz, CDCl₃): δ = 7.43–7.39 (m, 5H, arom.), 6.62–6.58 (m, 2H, isoquinoline), 6.44 (bs, 1H, NH: exch. with D₂O), 6.27 (d, 1H, J = 6.1 Hz, furanyl): 6.15 (d, 1H, J = 6.1 Hz, furyl), 4.61 (s, 1H, ArCHHNCO, conformer signal), 4.53 (s, 1H, ArCHHNCO, conformer signal), 3.85 (s, 6H, OCH₃), 3.77 (t, 1H, J = 5.8 Hz, ArCH₂CHHN, conformer signal), 3.65 (s, 2H, CH₂CONH, and t, 1H, J = 5.8 Hz, ArCH₂CHHN, conformers signals), 3.26 (q, 2H, J = 6.2 Hz, NHCH₂(CH₂)₃), 2.80 (t, 1H, J = 6.2 Hz, ArCHHCH₂N, conformer signal), 2.72 (t, 1H, J = 6.2 Hz, ArCHHCH₂N, conformer signal), 2.41 (t, 2H, J = 6.9 Hz, NH(CH₂)₃CH₂CO, conformer signal), 1.72–1.51 ppm (m, 4H, NHCH₂(CH₂)₂CH₂CO); ¹³C NMR (75 MHz, CDCl₃, conformers signals): δ = 171.75, 171.71, 166.4, 163.8, 152.8, 148.2, 148.1, 147.92, 147.89, 143.4, 138.9, 130.3, 129.1, 129.0, 128.6, 127.1, 125.9, 125.5, 124.3, 117.3, 114.4, 114.3, 111.79, 111.73, 111.39, 111.33, 109.6, 109.0, 108.3, 56.24, 56.14, 47.2, 44.1, 43.5, 39.8, 34.0, 33.0, 32.8, 29.2, 28.9,

1551, 1518, 1435, 1257, 1115, 941, 773, 701 cm⁻¹; ESI-MS (*m/z*): C₃₁H₃₂³⁷ClN₃O₆, 600 [*M* + H]⁺ (30), C₃₁H₃₂³⁵ClN₃O₆ 600 [*M* + H]⁺ (100).

2-[3,4-Bis(4-methoxyphenyl)isoxazol-5-yl]-N-[5-[6,7-dimethoxy-3,4-dihydroisoquinolin-2-(1*H*)-yl]-5-oxopentyl]acetamide (16): Compound 13 (200 mg, 0.61 mmol), HOBT (150 mg, 0.98 mmol), EDC·HCl (140 mg, 0.730 mmol), and drained DIPEA (134 mg, 1.04 mmol) were added to a solution of 2-[3,4-bis(4-methoxyphenyl)isoxazol-5-yl]acetic acid (mofezolac; 340 mg, 1.04 mmol) in dry DMF (10 mL) at room temperature. The reaction mixture was stirred overnight, then saturated aq. NaHCO₃ (20 mL) was added, and the aqueous solution was extracted with EtOAc (3 x 30 mL). The combined organic layers were washed with brine and dried over anhydrous sodium sulfate, and the solvent was evaporated under reduced pressure. The crude residue was purified by column chromatography on a silica gel column with CHCl₃/MeOH (95:5) and EtOAc as the mobile phases to give the target compound as

a white solid (150 mg, 40 % yield): mp: 90–92 °C; ¹H NMR (300 MHz, CDCl₃): δ = 7.42–7.38 (m, 2H, arom.), 7.19–7.15 (m, 2H, arom.), 6.95–6.88 (m, 2H, arom.), 6.82–6.78 (m, 2H, arom.), 6.62–6.57 (m, 2H,

isoquinoline), 6.38–6.25 (bs, 1H, NH: exch. with D₂O), 4.59 (slightly 28.2, 22.0, 21.9 ppm; FT-IR (KBr): $\tilde{\nu}$ = 3435, 2923, 2851, 1722, 1629,

broad singlet, 1 H, ArCHHNCO, conformer signal), 4.51 (slightly broad singlet, 1 H, ArCHHNCO, conformer signal), 3.83–3.73 (m, 13H, 4 OCH₃ and 1 H, ArCH₂CHHNCO, conformers signals), 3.68–3.58 (m, 3 H, ArCH₂CONH and ArCH₂CHHNCO, conformers signals), 3.27 (q, 2 H, *J* = 6.2 Hz, NHCH₂(CH₂)₃), 2.77 (t, 2 H, *J* = 5.8 Hz, ArCH-HCH₂NCO, conformer signal), 2.71 (t, 1 H, *J* = 5.8 Hz, ArCHHCH₂NCO, conformer signal), 2.40 (t, 1 H, *J* = 6.9 Hz, (CH₂)₃CH₂CON), 1.71–1.53 ppm (m, 4 H, CH₂(CH₂)₂CH₂); ¹³C NMR (75 MHz, CDCl₃, conformers signals): *d* = 171.80, 171.76, 167.0, 163.1, 161.2, 160.7, 159.6, 148.1, 148.0, 147.9, 147.8, 131.3, 130.0, 127.1, 126.0, 125.5, 124.4, 121.7, 121.4, 117.7, 114.5, 114.1, 111.77, 111.73, 111.42, 111.36, 109.6, 109.5, 109.1, 109.08, 56.2, 56.1, 55.5, 55.4, 47.2, 44.1, 43.5, 39.9, 39.7, 34.2, 33.2, 32.9, 29.2, 29.0, 28.2, 22.2, 22.1 ppm; FT-IR (KBr): $\tilde{\nu}$ = 3300, 3074, 3000, 2934, 2837, 1612, 1515, 1455, 1433, 1304, 1251, 1177, 1114, 1021, 967, 936, 836, 799, 750 cm⁻¹; ESI-MS (*m/z*): C₃₅H₃₉N₃O₇, 636 [*M*+Na]⁺.

2-[3,4-Bis(4-methoxyphenyl)isoxazol-5-yl]-1-[6,7-dimethoxy-3,4-dihydroisoquinolin-2-(1*H*)-yl]ethanone (17): 6,7-Dimethoxy-3,4-di-

hydroisoquinoline (50.2 mg, 0.26 mmol), HOBt (61 mg, 0.40 mmol), EDC·HCl (57.5 mg, 0.30 mmol), and dry DIPEA (58.1 mg, 0.023 mL, 0.45 mmol) were added to a solution of mofezolac (144 mg, 0.44 mmol) in dry DMF (14 mL) at room temperature. The reaction mixture was stirred for 24 h, then saturated aq. NaHCO₃ (20 mL) was added, and the aqueous solution extracted with EtOAc (3 x 30 mL). The combined organic layers were washed with brine and dried over anhydrous sodium sulfate, and the solvent was evaporated under reduced pressure. Column chromatography of the crude residue on silica gel with EtOAc as the mobile phase gave the target compound as a yellow solid (37.4 mg, 30 % yield): mp:

70–73 °C. ¹H NMR (300 MHz, CDCl₃): *d* = 7.42–7.35 (m, 2 H, arom.), 7.23–7.15 (m, 2 H, arom.), 6.91–6.78 (m, 4 H, arom.), 6.62–6.58 (m, 2 H, isoquinoline), 4.66 (s, 1 H, ArCHHNCO, conformer signal), 4.54 (s, 1 H, ArCHHNCO, conformer signal), 3.91–3.61 (m, 16 H, 4 OCH₃, ArCH₂CON and ArCH₂CH₂NCO), 2.82 (t, 1 H, *J* = 5.7 Hz, ArCH-HCH₂NCO, conformer signal), 2.75 ppm (t, 1 H, *J* = 5.7 Hz, ArCH-HCH₂NCO, conformer signal); ¹³C NMR (75 MHz, CDCl₃, conformers signals): *d* = 166.1, 165.9, 163.1, 161.1, 160.7, 159.6, 148.2, 148.1, 147.9, 131.5, 131.4, 130.1, 129.9, 126.9, 125.8, 125.0, 123.9, 122.0, 121.9, 121.5, 121.4, 117.6, 117.5, 114.4, 114.1, 111.75, 111.67, 111.40, 111.32, 109.56, 109.48, 109.0, 108.9, 56.3, 56.1, 55.7, 55.5, 47.9, 44.6, 44.3, 40.5, 32.3, 31.9, 29.1, 28.1 ppm; FT-IR (KBr): $\tilde{\nu}$ = 3069, 2997,

2935, 2836, 1651, 1610, 1574, 1516, 1363, 1112, 1024, 968, 902, 835 cm⁻¹; ESI-MS (*m/z*): C₃₀H₃₀N₂O₆, 537 [*M* + Na]⁺.

Methyl 5-[2-[1-(4-chlorobenzoyl)-5-methoxy-2-methyl-1 *H*-indol-3-yl]acetamido]pentanoate (18): DCC (144.2 mg, 0.7 mmol) and HOBt (81 mg, 0.6 mmol) were added to a stirred solution of indomethacin (100 mg, 0.5 mmol) in dry CH₂Cl₂ (10 mL) at 0 °C. DIEA (0.2 mL, 1.1 mmol) and methyl 5-aminopentanoate (100 mg, 0.6 mmol) in dry CH₂Cl₂ (10 mL) were then dropwise added at 0 °C. The reaction was stirred overnight at room temperature. The reaction mixture was then filtered, and the solvent was evaporated under reduced pressure. Column chromatography of the crude residue on silica gel and EtOAc/hexane (2:8) as a mobile phase afforded the target compound as a yellow solid (180 mg, 77 % yield); mp: 126–128 °C; ¹H NMR (300 MHz, CDCl₃): δ = 7.67 (d, 2H, *J* = 8.5 Hz, arom.), 7.48 (d, 2H, *J* = 8.5 Hz, arom.), 6.89–6.85 (m, 2H, arom.), 6.69 (dd, 1H, *J* = 9.0 and 2.5 Hz, arom.), 5.70–5.66 (bs, 1H, NH: exch. with D₂O), 3.82 (s, 3H, ArOCH₃), 3.63 (s, 2H, CH₂CONH), 3.62 (s, 3H, COOCH₃), 3.25–3.16 (m, 2H, NHCH₂(CH₂)₃), 2.38 (s, 3H, ArCH₃), 2.27 (t, 2H, *J* = 6.8 Hz, (CH₂)₃CH₂), 1.58–1.38 ppm (m, 4H, CH₂(CH₂)₂CH₂); ¹³C NMR (75 MHz, CDCl₃): δ = 174.0, 170.1, 168.6, 156.5, 139.8, 136.6, 133.8, 131.4, 131.1, 130.5, 129.4, 115.4, 113.1, 112.6, 100.9, 55.9, 51.8, 39.3, 34.1, 33.5, 32.5, 29.1, 25.8, 25.1, 22.0, 13.5 ppm; ESI-MS (*m/z*): C₂₅H₂₇N₂O₅, 469 (*M* – 1), 493 [*M* + Na]⁺.

5-[2-(5-Methoxy-2-methyl-1 *H*-indol-3-yl)acetamido]pentanoic acid (19):^[41] A solution of 0.5N LiOH (200 mg, 8 mmol, in 7 mL of H₂O) was added dropwise to a solution of 18 (170 mg, 0.362 mmol) in THF (5 mL) at room temperature. After 1.5 h, 1N HCl (18 mL) was added, and the aqueous phase was extracted with EtOAc (3 x 30 mL). The combined organic layers were dried over anhydrous sodium sulfate, and the solvent was evaporated under reduced pressure. Column chromatography of the crude residue on silica gel with EtOAc (100 %) to CHCl₃/CH₃OH (95:5) as the mobile phase afforded the target compound as a white solid (100 mg, 87 % yield); mp: 122–125 °C; ¹H NMR (300 MHz, [D₄]MeOH): δ = 7.50–7.35 (bs, 1H, NH: exch. with D₂O), 7.13 (d, 2H, *J* = 8.8 Hz, arom.), 6.90 (d, 2H, *J* = 2.3 Hz, arom.), 6.67 (dd, 1H, *J* = 8.8 and 2.3 Hz, arom.), 3.78 (s, 3H, OCH₃), 3.54 (s, 2H, CH₂CONH), 3.20–3.10 (m, 2H, NHCH₂), 2.34 (s, 3H, ArCH₃), 2.23 (t, 2H, *J* = 7.1 Hz, CH₂COOH), 1.58–1.40 ppm (m, 4H, CH₂(CH₂)₂CH₂); ¹³C NMR (75 MHz, CDCl₃): δ = 176.1, 173.8, 154.0, 134.3, 131.1, 128.9, 110.9, 110.3, 103.8, 99.7, 55.1, 38.9, 33.2, 31.7, 28.7, 22.0, 10.3 ppm; FT-IR (KBr): $\tilde{\nu}$ = 3403, 3292, 2924, 2854, 1699, 1622, 1540, 1488, 1463, 1434, 1355, 1311, 1203, 1111, 1037, 864, 668, 556 cm⁻¹.

N-{5-[6,7-Dimethoxy-3,4-dihydroisoquinolin-2-(1*H*)-yl]-5-oxopentyl}-2-(5-methoxy-2-methyl-1*H*-indol-3-yl)acetamide (20): DCC (338 mg, 1.64 mmol) and DMAP (36 mg, 0.296 mmol) were added to a stirred solution of 19 (265 mg, 0.83 mmol) in dry CH₂Cl₂ (20 mL) under argon atmosphere at 0 °C. After 30 min, a solution of 6,7-DM-THIQ (317 mg, 1.64 mmol) in dry CH₂Cl₂ (10 mL) was added dropwise at room temperature. The reaction mixture was stirred overnight, then 37 % HCl was added, and the aqueous solution was extracted with CH₂Cl₂. The combined organic phases were dried over anhydrous sodium sulfate, and the solvent was evaporated under reduced pressure. Column chromatography of the crude residue on silica gel using EtOAc/hexane (70:30) to CHCl₃/CH₃OH (97:3) as the mobile phase afforded the target compound as a yellow solid (409 mg, 23 % yield); mp: 57–60 °C; ¹H NMR (300 MHz, CDCl₃): δ = 8.10 (s, 1H, NH indole: exch. with D₂O), 7.17 (d, 1H, *J* = 8.8 Hz, arom.), 6.86 (s, 1H, arom.), 6.79 (dd, 1H, *J* = 8.8 and 2.4 Hz, arom.), 6.62–6.59 (m, 2H, isoquinoline), 5.84–5.81 (m, 1H, CONH: exch. with D₂O), 4.59 (s, 1H, ArCHHNCO, conformer signal), 4.49 (s, 1H, ArCHHNCO, conformer signal), 3.86–3.70 (m,

10H, 3 OCH₃ and ArCH₂CHHN, conformer signal), 3.60–3.56 (m, 3H, CH₂CONH and ArCH₂CHHN, conformer signal), 3.18 (q, 2H, *J* = 6.7 Hz, NHCH₂(CH₂)₃), 2.78 (t, 1H, *J* = 5.8 Hz, ArCHHCH₂N, conformer signal), 2.73 (t, 1H, *J* = 5.8 Hz, ArCHHCH₂N, conformer signal), 2.35–2.31 (m, 5H, ArCH₃ and CH₂CO-isoquinoline), 1.61–1.38 ppm (m, 4H, CH₂(CH₂)₂CH₂); ¹³C NMR (75 MHz, CDCl₃, conformers signals): δ = 171.8, 171.7, 154.5, 148.13, 148.06, 147.91, 147.87, 134.4, 130.6, 128.9, 127.1, 126.0, 125.5, 124.4, 111.7, 111.6, 111.5, 111.4, 109.5, 104.7, 100.0, 56.21, 56.16, 56.08, 47.2, 44.1, 43.5, 39.9, 39.2, 33.2, 32.9, 32.5, 29.4, 29.2, 28.2, 22.3, 22.2, 11.9; FT-IR (KBr): $\tilde{\nu}$ = 3298, 3069, 2933, 1640, 1518, 1486, 1455, 1362, 1311, 1257, 1217, 1114, 1031, 913, 853, 799, 753 cm⁻¹; ESI-MS (*m/z*): C₂₈H₃₅N₃O₅, 516 [*M* + Na]⁺.

Computational chemistry

Molecular modeling and graphics manipulations were performed using the molecular operating environment (MOE)^[42] and UCSF-CHIMERA^[43] software packages, running on a E4 Computer Engineering E1080 workstation with an Intel Core i7-930 Quad-Core processor. GOLD 5.2.2^[28,29] was used for all docking calculations. Figure were generated using PyMOL 1.0.^[44]

Ligand and receptor preparation: Model building and geometry optimization of compounds 8 and 17 was accomplished with the MMFF94X force field, available within MOE. The crystal structures of ovine COX-1 in complex with bound inhibitor indomethacin-(*R*)- α -ethyl-ethanolamide (PDB ID: 2OYE)^[27] and murine COX-2 complexed with SC-558 (PDB ID: 6COX)^[26] were used in the docking experiments, as the murine and ovine COX-2 sequences share a high level of identity (87.3 %). Database searching (SWISS-PROT), sequence alignment, and analysis of murine and ovine COX-2 sequences were carried out using the BLAST program.^[45] Moreover, all COX-2 active-site residues are largely conserved across the two species. Bound ligands and water molecules were removed. Correct atom assignment for Asn, Gln, and His residues was performed, and hydrogen atoms were added using standard MOE geometries. Partial atomic charges were computed by MOE using the Amber99 force field. All heavy atoms were then fixed, and hydrogen atoms were minimized using the Amber99 force field and a dielectric constant equal to 1, terminating at a gradient of 0.001 kcal mol⁻¹ Å⁻¹.

Docking simulations: Docking of 8 and 17 to COX-1 and COX-2, respectively, was performed using the GOLD software, which uses a genetic algorithm (GA) for determining the docking modes of ligands and proteins. The coordinates of the co-crystallized ligand (indomethacin-(*R*)- α -ethyl-ethanolamide for COX-1 and SC-558 for COX-2) were chosen as the active site origin. The active site radius was set to 10 Å. Mobility of the Arg 120, Tyr 355, Glu 524, and Ser 530 side chains was established using the flexible side chain option in the GOLD front end, which incorporates the Lovell rotamer library.^[46] Each GA run used the default parameters of 100 000 genetic operations on an initial population of 100 members divided into five subpopulations, with weights for crossover, mutation, and migration set to 95, 95, and 10, respectively. GOLD allows a user-definable number of GA runs per ligand, each of which starts from a different orientation. For these experiments, the number of GA runs was set to 200 without the option of early termination, and scoring of the docked poses was performed with the ChemPLP scoring function, followed by rescoring with ChemScore.^[3,19,30–34] The final receptor–ligand complex for each ligand was chosen interactively by selecting the highest scoring pose that

was consistent with experimentally derived information regarding the binding mode of the ligand.

Biology

Cyclooxygenase inhibition assays: The target compounds were evaluated for their ability to inhibit ovine COX-1 and COX-2 enzyme catalytic activity (percent inhibition at 50 μ M, unless otherwise indicated). IC₅₀ values were determined only for compounds that showed a reasonable COX-1 inhibitory activity (> 50 %) at 50 μ M (Table 2). Each reported IC₅₀ value and the percentage of inhibition (measured at 50 μ M as the tested compound concentration) is the average of the results of three separate assays (triplicate). Enzyme inhibition was determined using a colorimetric COX (ovine) inhibitor screening assay kit (Cayman Chemicals, Ann Arbor, MI, USA) following the manufacturer's instructions. Stock solutions of test compounds were dissolved in a minimum volume of DMSO.

Calcein-AM assays: Calcein-AM is a lipophilic pro-fluorescent probe and a P-gp substrate. In the presence of a P-gp inhibitor, calcein-AM is able to permeate the cell membrane and is hydrolyzed by cytosolic esterases to fluorescent calcein. As calcein is hydrophilic and is not a P-gp substrate, it cannot cross the cell membrane, and a rapid increase in fluorescence can be measured. These experi-

ments were carried out as previously described^[39] with minor modifications. Briefly, an MDCK-MDR1 cell line was seeded (50 000

cells per well) into black 96-well plates with 100 μ L of medium, and cells were allowed to become confluent overnight. Test compounds were solubilized in 100 μ L of culture medium and were added to the cell monolayers. The plates were then incubated at 37 °C for 30 min. Calcein-AM was added in 100 μ L of phosphate-buffered saline (PBS) to yield a final concentration of 2.5 μ M, and the plate was incubated for another 30 min. Each well was washed three times with ice-cold PBS. Saline buffer (100 μ L) was added to each well, and the plates were read with a Victor3 fluorimeter (PerkinElmer) at excitation and emission wavelengths of 485 and 535 nm, respectively. Under these experimental conditions, calcein cell accumulation in the absence and presence of tested compounds was evaluated, and basal-level fluorescence was estimated from the fluorescence of untreated cells. In treated wells, the increase in fluorescence was measured relative to that of the basal level. EC₅₀ values were determined by fitting the percent fluorescence increase versus log[dose].

Permeability assays: Caco-2 cells were harvested with trypsin-EDTA and seeded into a MultiScreen Caco-2 assay system at a density of 10 000 cells per well. The culture medium was replaced every 48 h for the first six days and every 24 h thereafter. After 21 days in culture, the Caco-2 cell monolayer was used for the permeability experiments. The transepithelial electrical resistance (TEER) of the monolayers was measured daily before and after the experiment using an epithelial voltohmmeter (Millicell-ERS; Millipore, Billerica, MA, USA). Generally, the obtained TEER values were greater than 1000 Ω for a 21-day culture.

Drug transport assays: The permeability assay allows two fluxes through the cell monolayer to be studied, from the basolateral to the apical (B \rightarrow A) and from the apical to the basolateral (A \rightarrow B) compartments, thus predicting the interacting mechanism of the tested compound with the efflux pump. In particular, if a studied compound is a P-gp inhibitor has an apparent permeability (P_{app}) BA/AB < 2, whereas a P-gp substrate shows BA/AB > 2.^[40] Apical to basolateral (P_{app} A \rightarrow B) and basolateral to apical (P_{app} B \rightarrow A) permeability of drugs were measured at 120 min at a concentration of

(HBSS, pH 7.4) and were sterile-filtered. After 21 days of cell growth, the medium was removed from filter wells and from the receiver plate. The filter wells were each filled with 75 μ L of fresh HBSS buffer and the receiver plate was filled with 250 μ L per well of the same buffer. This procedure was repeated twice, and the plates were incubated at 37 °C for 30 min. After incubation, the HBSS buffer was removed, and in some wells, drug solutions were added to the filter wells (75 μ L), and HBSS without drug was added to the corresponding receiver plate (250 μ L); in other wells, the drug solutions were added to the receiver plate (250 μ L), and HBSS without drug was added to the corresponding filter wells.

The plates were incubated at 37 °C for 120 min. After incubation, the samples were removed both from the apical (filter well) and basolateral (receiver plate) side of the monolayer and were stored at -20 °C pending analysis. The concentrations of compounds were analyzed using UV/Vis spectroscopy. The P_{app} , in units of $\text{cm}^2 \text{s}^{-1}$, was calculated using Equation (1):

$$P_{app} = \frac{1}{4} \frac{V_A}{\text{area}} \times \frac{t}{\Delta t} \times \frac{[drug]_{\text{acceptor}} - [drug]_{\text{init}}}{[drug]_{\text{init}}} \quad (1)$$

where V_A is the volume (μ L) in the acceptor well, area is the surface area of the membrane (0.11 cm^2 of the well), t is the total transport time in seconds (7200 s), $[drug]_{\text{acceptor}}$ is the concentration

of the drug as measured by UV spectroscopy, and $[drug]_{\text{init}}$ is the

100 μ M. Drugs were dissolved in Hank's balanced salt solution



Analytical methods: ESI-MS analyses were performed by 10 mL min^{-1} direct infusion of a MeOH sample solution on an Agilent 1100 LC-MSD trap system VL (ESI ion source type, 4 000 V ion source voltage). Samples from in vitro permeation studies were analyzed using a Shimadzu UV-1800 spectrophotometer. For each compound, a calibration curve was constructed at the opportune wavelength (Table 4).

Table 4. Absorption wavelength and molar extinction coefficient of each compound tested.

Compound	λ [nm]	ϵ [$\text{m}^{-1} \text{cm}^{-1}$]
8	230	44 725
15	280	8248
16	230	35 831
17	230	33 109

Statistical analysis: The IC_{50} and EC_{50} values of the compounds reported in Tables 2 and 3 were determined by nonlinear curve fitting using GraphPad Prism version 3.0 (GraphPad Software Inc., San Diego, CA, USA).^[47]

Acknowledgements

This work was supported financially by the Ministero dell'Istruzione, dell'Università e della Ricerca Scientifica e Tecnologica, Rome, Italy (MIUR-PRIN 2010-2011, prot. 2010W7YRLZ_003 to A.L.).

Keywords: molecular docking · decomposition analysis · cyclooxygenase · isoxazoles · P-glycoprotein

- [1] M. G. Perrone, A. Scilimati, L. Simone, P. Vitale, *Curr. Med. Chem.* 2010, **17**, 3769–3805.
- [2] C. Yuan, R. S. Sidhu, D. V. Kuklev, Y. Kado, M. Wada, I. Song, W. L. Smith, *J. Biol. Chem.* 2009, **284**, 10046–10055.
- [3] P. Vitale, M. G. Perrone, P. Malerba, A. Lavecchia, A. Scilimati, *Eur. J. Med. Chem.* 2014, **74**, 606–618.
- [4] M. G. Perrone, P. Vitale, A. Panella, C. G. Fortuna, A. Scilimati, *Eur. J. Med. Chem.* 2015, **94**, 252–264.
- [5] M. G. Perrone, P. Malerba, Md. J. Uddin, P. Vitale, A. Panella, B. C. Crews, C. K. Daniel, K. Ghebreselasie, M. Nickels, M. N. Tantawy, H. C. Manning, L. J. Marnett, A. Scilimati, *Eur. J. Med. Chem.* 2014, **80**, 562–568.
- [6] S. H. Choi, S. Aid, L. Caracciolo, S. S. Minami, T. Niikura, Y. Matsuoka, R. S. Turner, M. P. Mattson, F. Bosetti, *J. Neurochem.* 2013, **124**, 59–68.
- [7] R. Calvello, M. A. Panaro, M. L. Carbone, A. Cianciulli, M. G. Perrone, P. Vitale, P. Malerba, A. Scilimati, *Pharmacol. Res.* 2012, **65**, 137–148.
- [8] N. A. Colabufo, F. Berardi, M. Cantore, M. Contino, C. Inglese, M. Niso, R. Perrone, *J. Med. Chem.* 2010, **53**, 1883–1897.
- [9] P. Vitale, S. Tacconelli, M. G. Perrone, P. Malerba, L. Simone, A. Scilimati, A. Lavecchia, M. Dovizio, E. Marcantoni, A. Bruno, P. Patrignani, *J. Med. Chem.* 2013, **56**, 4277–4290.
- [10] J. J. Prusakiewicz, A. S. Felts, B. S. Mackenzie, L. J. Marnett, *Biochemistry* 2004, **43**, 15439–15445.
- [11] L. Di Nunno, P. Vitale, A. Scilimati, S. Tacconelli, P. Patrignani, *J. Med. Chem.* 2004, **47**, 4881–4890.
- [12] M. Kajitani, M. Tanaka, Y.-I. Hagiwara, M. Yasumoto (Taiho Pharmaceutical Co. Ltd.), US Pat. No. US5142091, 1992.
- [13] N. A. Colabufo, F. Berardi, M. G. Perrone, E. Capparelli, M. Cantore, C. Inglese, R. Perrone, *Curr. Top. Med. Chem.* 2010, **10**, 1703–1714.
- [14] K. McHugh, R. Callaghan, *Multidrug Resistance: Biological and Pharmaceutical Advances in Antitumor Treatment* (Ed.: N. A. Colabufo), Research Signpost, Kerala, India, 2008.
- [15] E. Capparelli, L. Zinzi, M. Cantore, M. Contino, M. G. Perrone, G. Luurtsema, F. Berardi, R. Perrone, N. A. Colabufo, *J. Med. Chem.* 2014, **57**, 9983–9994.
- [16] M. Contino, L. Zinzi, M. Cantore, M. G. Perrone, M. Leopoldo, F. Berardi, R. Perrone, N. A. Colabufo, *Bioorg. Med. Chem. Lett.* 2013, **23**, 3728–3731.
- [17] M. Arisawa, Y. Kasaya, T. Obata, T. Sasaki, T. Nakamura, T. Araki, K. Yamamoto, A. Sasaki, A. Yamano, M. Ito, H. Abe, Y. Ito, S. Shuto, *J. Med. Chem.* 2012, **55**, 8152–8163.
- [18] A. Angelini, M. Iezzi, C. Di Febbo, C. Di Ilio, F. Cuccurullo, E. Porreca, *Oncol. Rep.* 2008, **20**, 731–735.
- [19] M. G. Perrone, P. Vitale, P. Malerba, A. Altomare, R. Rizzi, A. Lavecchia, C. Di Giovanni, E. Novellino, A. Scilimati, *ChemMedChem* 2012, **7**, 629–641.
- [20] M. G. Perrone, D. Lofrumento, P. Vitale, F. De Nuccio, V. La Pesa, A. Panella, R. Calvello, A. Cianciulli, M. A. Panaro, A. Scilimati, *Pharmacology* 2015, **95**, 22–28.
- [21] Md. J. Uddin, B. C. Crews, K. Ghebreselasie, L. J. Marnett, *Bioconjugate Chem.* 2013, **24**, 712–723.
- [22] Md. J. Uddin, B. C. Crews, A. L. Blobaum, P. J. Kingsley, D. L. Gorden, J. O. McIntyre, M. L. Matrisian, K. Subbaramaiah, A. J. Dannenberg, D. W. Piston, L. J. Marnett, *Cancer Res.* 2010, **70**, 3618–3627.
- [23] M. A. Cinelli, B. Cordero, T. S. Dexheimer, Y. Pommier, M. Cushman, *Bioorg. Med. Chem.* 2009, **17**, 7145–7155.
- [24] L. Huang, F.-p. Hou, P. Xi, D. Bai, M. Xu, Z. Li, G. Xie, Y. Shi, H. Liu, Z. Zeng, *J. Inorg. Biochem.* 2011, **105**, 800–805.
- [25] I. Carlescu, H. M. I. Osborn, J. Desbrieres, D. Scutaru, M. Popa, *Carbohydr. Res.* 2010, **345**, 33–40.
- [26] R. G. Kurumbail, A. M. Stevens, J. K. Gierse, J. J. McDonald, R. A. Stegeman, J. Y. Pak, D. Gildehaus, J. M. Miyashiro, T. D. Penning, K. Seibert, P. C. Isakson, W. C. Stallings, *Nature* 1996, **384**, 644–648.
- [27] C. A. Harman, M. V. Turman, K. R. Kozak, L. J. Marnett, W. L. Smith, R. M. Garavito, *J. Biol. Chem.* 2007, **282**, 28096–28105.
- [28] GOLD version 5.2.2, CCDC Software Ltd., Cambridge (UK), 2008.
- [29] G. Jones, P. Willett, R. C. Glen, A. R. Leach, R. Taylor, *J. Mol. Biol.* 1997, **267**, 727–748.
- [30] M. L. Verdonk, J. C. Cole, M. J. Hartshorn, C. W. Murray, R. D. Taylor, *Proteins Struct. Funct. Genet.* 2003, **52**, 609–623.
- [31] N. Micale, R. Ettari, A. Lavecchia, C. Di Giovanni, K. Scarbaci, V. Troiano, S. Grasso, E. Novellino, T. Schirmeister, M. Zappalà, *Eur. J. Med. Chem.* 2013, **64**, 23–34.
- [32] G. Fracchiolla, A. Laghezza, L. Piemontese, P. Tortorella, F. Mazza, R. Montanari, G. Pochetti, A. Lavecchia, E. Novellino, S. Pierno, D. Conte Camerino, F. Loidice, *J. Med. Chem.* 2009, **52**, 6382–6393.
- [33] L. Porcelli, F. Gilardi, A. Laghezza, L. Piemontese, N. Mitro, A. Azzariti, F. Altieri, L. Cervoni, G. Fracchiolla, M. Giudici, U. Guerrini, A. Lavecchia, R. Montanari, C. Di Giovanni, A. Paradiso, G. Pochetti, G. M. Simone, P. Tortorella, M. Crestani, F. Loidice, *J. Med. Chem.* 2012, **55**, 37–54; G. Fracchiolla, M. Giudici, U. Guerrini, A. Lavecchia, R. Montanari, C. Di Giovanni, A. Paradiso, G. Pochetti, G. M. Simone, P. Tortorella, M. Crestani, F. Loidice, *J. Med. Chem.* 2012, **55**, 37–54.
- [34] K. Scarbaci, V. Troiano, N. Micale, R. Ettari, C. Di Giovanni, C. Cerchia, S. Grasso, E. Novellino, T. Schirmeister, A. Lavecchia, M. Zappalà, *Eur. J. Med. Chem.* 2014, **76**, 1–9.
- [35] A. J. Vecchio, D. M. Simmons, M. G. Malkowski, *J. Biol. Chem.* 2010, **285**, 22152–22163.
- [36] K. Gupta, B. S. Selinsky, C. J. Kaub, A. K. Katz, P. J. Loll, *J. Mol. Biol.* 2004, **335**, 503–518.
- [37] E. D. Thuresson, K. M. Lakkides, C. J. Rieke, Y. Sun, B. A. Wingerd, R. Micelli, A. M. Mulichak, M. G. Malkowski, R. M. Garavito, W. L. Smith, *J. Biol. Chem.* 2001, **276**, 10347–10357.
- [38] O. Llorens, J. J. Perez, A. Palomer, D. Mauleon, *Bioorg. Med. Chem. Lett.* 1999, **9**, 2779.
- [39] B. Feng, J. B. Mills, R. E. Davidson, R. J. Mireles, J. S. Janiszewski, M. D. Troutman, S. M. de Moraes, *Drug Metab. Dispos.* 2008, **36**, 268–275.
- [40] J. W. Polli, S. A. Wring, J. E. Humphreys, L. Huang, J. B. Morgan, L. O. Webster, C. S. Serabjit-Singh, *J. Pharmacol. Exp. Ther.* 2001, **299**, 620–628.
- [41] T. Y. Shen, L. R. Ellis, T. B. Windholz, A. R. Matzuk, A. Rosegay, S. Lucas, B. E. Witzel, C. H. Stammer, A. N. Wilson, F. W. Holly, J. D. Willett, L. H. Sarett, W. J. Holtz, *J. Am. Chem. Soc.* 1963, **85**, 488–489.
- [42] Molecular Operating Environment (MOE) version 2013.08, Chemical Computing Group Inc., 1010 Sherbooke St. West, Suite #910, Montreal, QC, H3A 2R7 (Canada), 2012.
- [43] C. C. Huang, G. S. Couch, E. F. Pettersen, T. E. Ferrin, *Pac. Symp. Biocomput.* 1996, **724**, <http://www.cgl.ucsf.edu/chimera>.
- [44] W. L. DeLano, The PyMOL Molecular Graphics System, DeLano Scientific LLC, San Carlos, CA (USA), <http://www.pymol.org/>.
- [45] Y. J. Pak, S. Wang, *J. Phys. Chem. B* 2000, **104**, 354–359.
- [46] S. C. Lovell, J. M. Word, J. S. Richardson, D. C. Richardson, *Proteins Struct. Funct. Bioinf.* 2000, **40**, 389–408.
- [47] Prism version 3.0 for Windows, GraphPad Software Inc., San Diego, CA (USA), 1998.